Frenkel excitons in the disordered system,
and their optical nonlinear response
around the localized-delocalized transition

（ランダム系のフレンケル励起子と
　　局在-非局在転移付近における光非線形応答）

Nobuhiko Taniguchi

（谷 口 伸 彦）

Thesis

Frenkel excitons in the disordered system, and their optical nonlinear response around the localized-delocalized transition

（ランダム系のフレンケル励起子と
局在-非局在転移付近における光非線形応答）

Nobuhiko Taniguchi
（ 谷 口 伸 彦 ）

Department of Applied Physics, University of Tokyo,
Hongo, Bunkyo-ku, Tokyo 113 Japan

Contents

Chapter 1

Introduction

1.1 Introduction

This thesis is devoted to the theoretical study of optical linear and nonlinear responses in the disordered system. We are concerned mainly with optical nonlinear responses due to excitons. Exciton systems are very promising as a nonlinear material (Sec. 1.2). Roughly speaking, it is because an exciton has an enhanced transition dipolemoment, *i.e.*, the ability to interact collectively with the radiation field (Sec. 1.3). An *effective* value of the enhanced transition dipolemoment is determined approximately by a spread of the exciton's wavefunction, which must have close relation to the relaxation mechanism of an exciton. However, such evaluation of optical nonlinear responses only by the effective transition dipolemoment with the use of the relaxation times T_1 and T_2 is too crude to give an interesting phenomena such as the weak localization effect on the phase-conjugated wave generation (Sec. 1.4). The third-order nonlinear process generating the phase-conjugated wave will be found to be very sensitive to the interference caused by the exciton's scattering with static disorder in the system. So as to treat the exciton's coherency properly, the microscopic mechanism of relaxation is needed. When we use a random potential model as a microscopic description of the dephasing process, the problem of the Anderson localization will emerge (Sec. 1.5). It allures us to construct the scaling theory of the phase-conjugated wave generation. We will find that various topics in different field correlate organically with one another. In Sec. 1.6, we will state the purpose and the outline of the thesis in a more specific way.

1.2 Excitons and Optical Nonlinear Responses

Optical nonlinear responses of solids have been studied extensively so far. However, many fundamental problems remain to be understood. The third-order optical nonlinear susceptibility $\chi^{(3)}$ describes a wide range of interesting optical nonlinear phenomena such as the four-wave mixing experiment and the generation of phase-conjugated waves (PCW) as well as optical bistability. In designing optoelectronic or optical devices, both of the large optical nonlinear susceptibility $\chi^{(3)}$ and the fast switching time τ are desired. Unfortunately these two properties don't seem to be compatible. If we define the figure of merit for the optical nonlinear material by $|\chi^{(3)}|/\alpha\tau$, where α is the absorption coefficient, an empirical law of $|\chi^{(3)}|/\alpha\tau \approx$ const. holds good in a large class of optical nonlinear materials. As Fig. 1.1 illustrates, only exceptions of this empirical law are exciton systems under resonant pumping. From this point of view, there is increasing interest in the nonlinear optical properties due to excitons in the organic and inorganic crystals. (See also, *e.g.*, Ref. [1].) Exciton systems are so promising as optical nonlinear materials that both the large optical nonlinearity and rapid switching will be realized in those systems.

1.3 Enhanced Dipolemoment and Nonlinear Responses

Such favorable properties of exciton systems as optical nonlinear materials result from collective interactions with the radiation field and it can be explained in terms of the enhanced oscillator strength of an exciton. If we designate an annihilation (creation) operator of the valence (conduction) electron in the state of the Wannier function at the site r_i, the general exciton states $|\Psi_{\lambda n}\rangle$ can be

expressed by

$$|\Psi_{\lambda n}\rangle = \sum_{i,j} F_{\lambda n}(\boldsymbol{R})\,\varphi_n(\boldsymbol{r})\,b_i^\dagger a_j|g\rangle, \tag{1}$$

where the coordinate $\boldsymbol{R}$ ($\boldsymbol{r}$) is a center-of-mass (relative) coordinate of the electron-hole pair at $\boldsymbol{r}_i$ and $\boldsymbol{r}_j$, and $F_{\lambda n}(\boldsymbol{R})$ ($\varphi_n(\boldsymbol{r})$) is a wavefunction of center-of-mass (relative) motion for the e-h pair. The suffix of the wavefunction λ (n) is a quantum number of the center-of-mass (relative) motion of the exciton. The transition dipolemoment between this state and the ground state is given by

$$\langle\Psi_{\lambda n}|\hat{\boldsymbol{P}}_K|g\rangle = \boldsymbol{\mu}\left[\sum_i F_{\lambda n}^*(\boldsymbol{R}_i)\,e^{i\boldsymbol{K}\cdot\boldsymbol{R}_i}\right]\varphi_n^*(\boldsymbol{r}=0). \tag{2}$$

The atomic dipolemoment is designated by $\boldsymbol{\mu}$, and $\hat{\boldsymbol{P}}_K = \boldsymbol{\mu}\sum_i(b_i^\dagger a_i + a_i^\dagger b_i)\,e^{i\boldsymbol{K}\cdot\boldsymbol{R}_i}$ is a Fourier component of the transition dipolemoment of the system.

Take Frenkel-type excitons as an example. Frenkel excitons are collective excitations, say, in the molecular crystal. Frenkel excitons correspond to the case of $\varphi_n(\boldsymbol{r}_i-\boldsymbol{r}_j)=\delta_{i,j}$ in Eq. (1). If there are no dephasing processes such as lattice vibration and scattering by defects in the crystal, the momentum of the center-of-mass motion $\boldsymbol{k}$ becomes a good quantum number. Then the wavefunction of the center-of-mass motion $F_{kn}(\boldsymbol{R}_i)$ is in the ideal crystal given by

$$F_{kn}(\boldsymbol{R}_i) = \frac{1}{\sqrt{N}}\,e^{i\boldsymbol{k}\cdot\boldsymbol{R}_i}. \tag{3}$$

The transition dipolemoment of this ideal Frenkel exciton becomes $\sqrt{N}$ times as large as the atomic dipolemoment $\boldsymbol{\mu}$:

$$\langle\psi_k|\hat{\boldsymbol{P}}_K|g\rangle = \sqrt{N}\,\boldsymbol{\mu}\,\delta_{k,K}. \tag{4}$$

In the case of Frenkel exciton localized with a localization length ξ_{loc}, $F_{\lambda n}(\boldsymbol{R}_i)$

behaves exponentially such as $F_{\lambda n}(\boldsymbol{R}_i) \approx \sqrt{a^3/\xi_{\text{loc}}^3} \exp(-R_i/\xi_{\text{loc}})^*$. The transition dipolemoment of this localized Frenkel exciton is also enhanced from the atomic value as

$$\langle \psi_{\text{loc}} | \hat{\boldsymbol{P}}_{\boldsymbol{K}} | g \rangle \approx \sqrt{\xi_{\text{loc}}^3/a^3} \, \boldsymbol{\mu}, \tag{5}$$

for $\boldsymbol{K} \approx \boldsymbol{0}$, when the localization length ξ_{loc} is much larger than the size of the unit cell a.

Since the third-order nonlinear polarization $\boldsymbol{P}^{(3)}$ is proportional to the transition dipolemoment to the fourth power[†], Eq. (4) shows that $\boldsymbol{P}^{(3)}$ due to ideal Frenkel excitons will be expected to scale as $\sim N^2$, not as $\sim N$. This means that the nonlinear susceptibility $\chi^{(3)}$, which is determined by the polarization density, has an enhancement factor of N due to the exciton's spatial coherence over the whole crystal. On the other hand, $\chi^{(3)}$ due to localized excitons should have an enhancement factor of $\sim \xi_{\text{loc}}^3/a^3$, as shown by Eq. (5). This simplified argument above will be found later to hold true only under resonant pumping of the exciton.

In a system of semiconductor of microcrystallites, the coherent size is determined by the sample size itself, which leads to the third-order susceptibility proportional to the volume of the semiconductor microcrystallite under resonant pumping of excitons [2–5]. If the momentum and energy relaxation of the exciton exist, these processes limit the coherent size[‡‡]. Consequently the factor N in

---

* The prefactor is necessary for the normalization condition of the wavefunction.
† The estimation of optical nonlinear responses here is oversimplified. In later chapters, we will confirm that it is true under certain conditions.
‡‡ The localization length of the exciton can also be considered a kind of the exciton's coherent length.

the enhancement factor of $\chi^{(3)}$ should be replaced by a smaller value N_{eff}. Unfortunately such relaxation processes are usually taken account of only phenomenologically by introduction of the longitudinal and transverse relaxation times T_1 and T_2. Such approximation is too crude to take serious account of the effect of intersite coherence on the nonlinear susceptibility. To examine the exciton's intersite coherent effect on optical nonlinear responses, the microscopic relaxation mechanism is needed. In fact, as will be seen in the next section, it is not until we use the microscopic model of static random onsite energies as a dephasing processes that we will find the peculiarity of the phase-conjugation in the random system. We also note that the exciton's coherent effect is not correctly treated within the framework of the local-field approximations, and simple-minded equation of motion method as in Ref. [6].

1.4 Phase-conjugated Waves and Weak Localization Effect

The generation of the phase-conjugated wave is a kind of optical nonlinear responses described by the third-order susceptibility $\chi^{(3)}$. The geometry of three incident beams — the forward and backward pump beams and the probe beam — is depicted in Fig. 1.2. When an exciton is scattered elastically by random potentials, it suffers from the momentum relaxation. These scattering processes make the motion of an exciton partially coherent and partially incoherent (*i.e.*, diffusive), and thus the effective dipolemoment of an exciton will be reduced [7,8].

The disorder effect not only reduces the transition dipolemoment, but also give a very interesting positive contribution to optical nonlinear responses. In

random systems, the backward scattering amplitude is known to be enhanced due to interference effect. In other words, the probability that a particle or an elementary excitation such as an exciton returns to the original point will increase, and the system is inclined to be localized. The importance of coherent multiple scattering by static random potentials has recently been recognized in nonlinear optical properties. Weak localization effect by disorder has been shown to enhance the generation of the phase-conjugated waves in nearly degenerate four-wave mixing [9–14]. They discussed and showed by the perturbational calculation that coherent collision due to random potentials enhances the strength of the phase-conjugated wave signal. (See also Ref. [15,16].) In the end of Chapter 4, we will explain intuitively how the coherent collision enhances the generation of the phase-conjugated wave.

When disorder in the system increases further, the localized-delocalized transition will occur and the exciton state will be localized. The weak localization effect is just a precursor of the localized state. Although the weak localization effect can be treated by the perturbational calculation from the delocalized limit, the same sort of calculation cannot be applied around the localized-delocalized transition. This topic will be argued more in the next section.

1.5 Anderson Localization

When disorder in the system increases further, the delocalized-localized transition (*i.e.*, Anderson transition) is expected to occur as a function of the strength of disorder, or of the frequency. Such transition point in the frequency domain is called mobility edge ω^*, where the states of the exciton change in

nature from the localized to the extended states or *vice versa*. The possibility of the localized-delocalized transition of the exciton [17–21] gives an interesting but nontrivial problem on optical nonlinear responses due to excitons. Since the exciton's localization length diverges when pump and probe frequencies approach the exciton mobility edge in the localized phase, the effective transition dipolemoment of an exciton should become very large near the transition point. Does this imply that the optical nonlinear responses will also become very large around the exciton mobility edge? It is noted that the exciton wave number is not a good quantum number in this system, so that linear absorption spectrum due to the exciton is very broad and almost constant around the mobility edge.

As for the Anderson localization of conductors (*i.e.*, electrons), there exists a very powerful theory — the scaling theory of the Anderson localization [22,23]. According to the scaling argument of the Anderson localization, all the states are localized in one- and two-dimensional bulk system at the absolute zero temperature, and the localized-delocalized transition is expected to occur as a function of disorder, or of frequency in the three-dimensional system. The dimensionality of the system is known to be a crucial parameter in the theory of the Anderson localization.

However no strong dependence on the dimensionality is manifested in the result of the weak localization effect on the phase-conjugated wave so far. In addition, the simple-minded estimation in the localized phase such as we set the diffuson coefficient to zero seems to give a wrong answer to the generation of the phase-conjugated signal in the localized phase. Commonly used methods such as perturbational calculation of exciton scattering by random potential break down,

particularly, around the exciton mobility edge. If we develop the length-dependent scaling theory for the phase-conjugated wave generation, we examine systematically its behavior on both the localized and the delocalized sides of the exciton mobility edge. Here we need the application of the scaling theory on the phase-conjugated wave generation.

Complicating the situation furthermore, both the restricted geometry of the sample and the misalignment of forward and backward pump beams also destroy the interference effect — the localization effect. In other words, both smear out the critical behavior around the transition point. To investigate such singular behavior in nonlinear polarization around the exciton mobility edge, the scaling theory of localization will be found very effective.

1.6 Purpose and Outline of the Thesis

The present thesis is devoted to the study of the disordered effect on the optical nonlinear polarization, particularly on the generation of the phase-conjugated wave. As we have seen in the previous sections, it is because the phase-conjugated wave generation is sensitive to disorder and gives us a particular interest in the random system. Although the exciton system is a very promising as an optical nonlinear material because of the exciton's intersite coherency itself, it is not fully understood yet from the microscopic point of view how the exciton's coherence contributes to optical nonlinear processes such as the generation of the phase-conjugated wave. The localized-delocalized transition of the exciton gives a very interesting situation, because the third-order nonlinear susceptibility $\chi^{(3)}$ is sensitive to a spread of the wavefunction. (On the other

hand, the liner susceptibility $\chi^{(1)}$ is not so sensitive to a spread of the wavefunction.) A certain kind of optical nonlinear responses ought to be enhanced around the exciton mobility edge.

Based upon these subjects introduced above, the following points will be clarified in the thesis: (1) How is the enhancement factor N_{eff} due to the exciton's coherency calculated from the microscopic model? (2) What singular behavior of the phase-conjugated signal is expected around the exciton mobility edge? (3) And how is the enhancement effect of the phase-conjugated signal destroyed by many factors, *i.e.*, the restricted geometry of the sample, the misalignment of the two pump beams, and the detuning frequency ?

We clarify the nature of phase-conjugated wave generation in the disordered and finite system, and its behavior around the localized-delocalized transition. Putting it the other way round, localization and delocalization of the exciton, which is still an open problem, can be studied well by observing the generation of phase-conjugated waves, when the pump and probe beam frequencies are close to the exciton mobility edge.

The outline of the thesis is as follows. We investigate the microscopic model of the exciton system in Chapter 2. We start from the microscopic Hamiltonian of Frenkel excitons with static onsite disorder. Dephasing processes of the exciton are included through the scattering by onsite disorder. The longitudinal damping of an exciton into the ground state is included phenomenologically in the form of the Liouville operator. In Chapter 3, we formulate linear optical response and nonlinear polarizations for phase-conjugated wave generation, taking full account of the disorder effect. In Chapter 4 we first

examine the dominant contribution for the third-order susceptibility under nearly resonant pumping of excitons. Next we perform the perturbational expansion from the delocalized limit. The relation between the enhancement factor for the phase-conjugated wave generation and the cooperon mode is explicitly shown. In Chapter 5, we develop the length-dependent scaling theory for the enhancement factor of the phase-conjugated wave generation. The spectral anomaly of this signal around the exciton mobility edge is demonstrated. Its dependence on the system size and the misalignment is also examined. In the final chapter, we summarize our results: the singular behavior of the phase-conjugated wave generation around the exciton mobility edge. We also discuss how to observe the localized-delocalized transition in frequency by observing the phase-conjugated wave generation as a function of pump frequency or of misalignment of two pump beams.
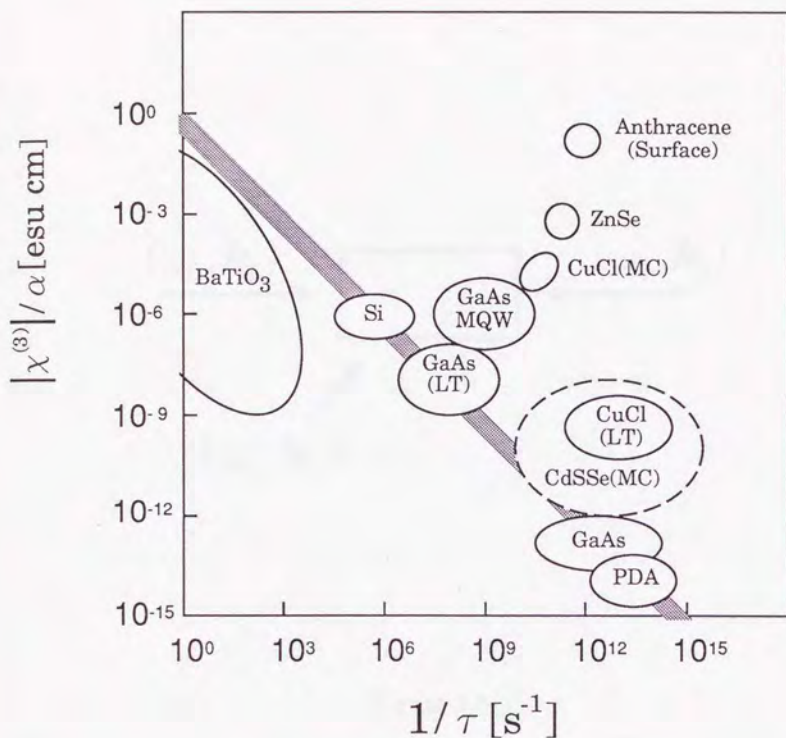
Figure 1.1

Logarithmic plotting of $|\chi^{(3)}|/\alpha$ as a function of $\log[1/\tau]$, where α is the absorption coefficient and τ is the switching time. The empirical law of $|\chi^{(3)}|/\alpha\tau = $ const. is drawn by the gray line in the figure. Exciton systems under resonant pumping are shown to be free from this empirical law, and be promising as optical nonlinear materials.

$(\omega_0, \boldsymbol{k}_f)$ $(\omega_0, \boldsymbol{k}_b)$

$(\omega_p, \boldsymbol{k}_p)$
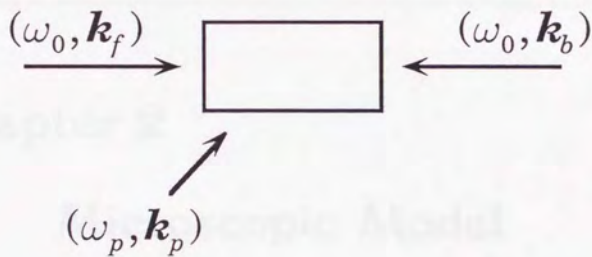
Figure 1.2

The geometry of the nearly degenerate four-wave mixing. Three incident beams are used: the forward (backward) pump beams denoted by $(\omega_0, \boldsymbol{k}_{f(b)})$, and the probe beam by $(\omega_p, \boldsymbol{k}_p)$. The signal beam which is phase-conjugated to the probe light is observed at $(\omega_s, \boldsymbol{k}_s) = (2\omega_0 - \omega_p, \boldsymbol{k}_f + \boldsymbol{k}_b - \boldsymbol{k}_p)$.

2.1 Outlook for Constructing a Microscopic Model

Chapter 2
Microscopic Model

2.1 Criteria for Constructing a Microscopic Model

In this chapter, we construct the microscopic model of Frenkel excitons in the disordered system which is appropriate to estimate optical nonlinear susceptibilities. As we have seen in the previous chapter, the microscopic model for the exciton's relaxation processes is needed when we take account of the exciton's coherency seriously to estimate the nonlinear susceptibility. It is our central interest to learn how the exciton's coherency affects various kinds of optical nonlinear responses. To treat the exciton system, the attractive interaction between an electron and a hole is needed. In addition, the system is not in equilibrium state when we observe optical nonlinear responses. Everything considered, such system is too complicated for us to deal with. Some simplifications in the model are needed.

Our first simplification is to treat the model of Frenkel excitons. In this model, the lowest exciton state is assumed to have so localized a wavefunction in the *relative* motion of the electron-hole pair that a pair of an electron and a hole are almost located at the same atom (or molecule). The exciton's coherency is defined by a spread of the wavefunction of the center-of-mass motion. This model has a merit of mathematical simplicity and, at the same time, allows us to examine the coherent effect on optical nonlinear susceptibilities.

As our second simplification, we take the situation where the relaxation of an exciton's momentum is much faster than that of an exciton's energy. From this assumption, we have only to use a microscopic mechanism for dephasing processes, *i.e.*, relaxation processes for an exciton's momentum. The distribution of static onsite random energies is introduced. This model gives excitons not

only the pure dephasing processes but also the weak localization effect which leads to the localized-delocalized transition, as we have mentioned in Chapter 1. Longitudinal relaxation processes, *i.e.*, relaxation processes of an exciton's energy, is treated only phenomenologically by assuming a tractable but plausible form of the Liouville operator*.

Optical nonlinear responses (and susceptibilities) can be estimated in a nonequilibrium system by help of the density matrix ϱ whose evolution obeys the Liouville equation. The details of this calculation will be presented in Chapter 3, where we will estimate nonlinear responses under a rotating wave approximation.

2.2 Microscopic Model for Optical Nonlinear Responses

2.2.1 Time evolution of the density matrix

We introduce the microscopic model for Frenkel excitons in N coupled two-level atoms (or molecules) with random onsite energies Ω_i and dipolar couplings between them. The ground state, the one-exciton states and the two-exciton states are depicted in Fig. 2.1. The volume of the system is defined as $V = L^d$ (L is a system size in dimension d). The time evolution of the density matrix $\varrho(t)$ of the electronic system is determined by the following Liouville equation (we use the unit of $\hbar = 1$ here and hereafter):

$$\frac{d\varrho}{dt} = -i[H_0 + H'(t), \varrho] + \mathcal{L}_\gamma \varrho, \tag{1}$$

---

* This is described by the Liouville operator $\mathcal{L}_\gamma \varrho$ in Eq. (1).

where H_0 is the Hamiltonian of electronic system and $H'(t)$ is the interaction between the electronic system and the transverse electric fields $\boldsymbol{E}^{\perp}(\boldsymbol{r},t)$. The term $\mathcal{L}_\gamma \varrho$ describes a longitudinal relaxation, *i.e.*, a relaxation of an exciton's energy, and its detailed form will be given later. In terms of a Pauli spin operator S_i^+ (S_i^-) creating (annihilating) an excitation at the site i, the Hamiltonians H_0 and $H'(t)$ are expressed by

$$H_0 = \sum_{(i,j)} T(\boldsymbol{r}_i - \boldsymbol{r}_j) S_i^+ S_j^-, \tag{2a}$$

$$H'(t) = -\int d\boldsymbol{r} \, \hat{\boldsymbol{P}}(\boldsymbol{r}) \cdot \boldsymbol{E}^{\perp}(\boldsymbol{r},t). \tag{2b}$$

The polarization density operator $\hat{\boldsymbol{P}}(\boldsymbol{r})$ is given by

$$\hat{\boldsymbol{P}}(\boldsymbol{r}) = \sum_i \boldsymbol{\mu}(S_i^+ + S_i^-)\delta(\boldsymbol{r} - \boldsymbol{r}_i), \tag{3}$$

with $\boldsymbol{\mu}$ the atomic transition dipolemoment.

2.2.2 Experimental Geometry for Phase-Conjugated Wave Generation

In the thesis, we consider mainly the phase-conjugated wave generation by the nearly degenerate four-wave-mixing experiment. The experimental setting is shown in Fig. 1.2. The two pump waves $(\omega_0, \boldsymbol{k}_f)$ and $(\omega_0, \boldsymbol{k}_b)$, and the probe wave $(\omega_p, \boldsymbol{k}_p)$ are applied on the optical nonlinear material. Thus the external electric field is expressed in the composition of three incident beams as

$$\boldsymbol{E}^{\perp}(\boldsymbol{r},t) = \sum_{l=1}^{3} \left(\boldsymbol{E}_l e^{i\boldsymbol{k}_l \cdot \boldsymbol{r} - i\omega_l t} + \boldsymbol{E}_l^* e^{-i\boldsymbol{k}_l \cdot \boldsymbol{r} + i\omega_l t} \right), \tag{9}$$

where $(\omega_l, \boldsymbol{k}_l)$ ($l = 1,2,3$) denote the forward $(\omega_0, \boldsymbol{k}_f)$, the backward $(\omega_0, \boldsymbol{k}_b)$ pump beams and the probe beam $(\omega_p, \boldsymbol{k}_p)$. Under a rotational wave approximation, we have three kinds of signal waves from the three kinds of population gratings, as

will be depicted later in Chapter 4. Among them, we observe the signal beam phase-conjugated to the incident probe light at $(\omega_s, \boldsymbol{k}_s) = (2\omega_0 - \omega_p, \boldsymbol{k}_f + \boldsymbol{k}_b - \boldsymbol{k}_p)$.

2.2.3 Random Configuration Average

The term $T(\boldsymbol{r}_i - \boldsymbol{r}_j)$ in the Hamiltonian H_0 describes the random onsite energy Ω_i for $i = j$ and the dipolar couplings for $i \neq j$. The onsite energies Ω_i are assumed to obey the Gaussian probability distribution

$$P[\Omega_i] = \prod_i \frac{1}{\sqrt{2\pi W^2}} \exp\left[-\frac{(\Omega_i - \Omega_0)^2}{2W^2}\right]. \tag{4}$$

Observed physical quantities must be evaluated, by averaging over the distribution of random onsite energies. This procedure is designated by

$$\langle \cdots \rangle_{av} \equiv \int \prod_i P[\Omega_i] d\Omega_i \, (\cdots). \tag{5}$$

From the definition of the distribution, the average and the variance of the onsite energies are given by

$$\langle \Omega_i \rangle_{av} = \Omega_0, \tag{6a}$$

$$\langle \Omega_i \Omega_j \rangle_{av} - \langle \Omega_i \rangle_{av} \langle \Omega_j \rangle_{av} = W^2 \delta_{i,j}. \tag{6b}$$

When we evaluate the nonlinear response by perturbational method in the later chapters, we explicitly assume that random onsite energies obey this Gaussian distribution. However, the behavior of the phase-conjugated wave signal which is obtained from the scaling theory is believed to be universal around the exciton mobility edge, irrespective of the Gaussian, box-type, or Lorentzian distribution of the random onsite energies.

2.2.4 Liouville operator for a Longitudinal Relaxation

The term $L_\gamma \varrho$ in the Liouville Eq. (1) describes the longitudinal relaxation of an exciton, *i.e.*, the relaxation processes of excited states into the ground state. Since we are concerned mainly with the disorder effect and such situation as the dephasing rate is much faster than the longitudinal relaxation rate, we introduce a constant decay rate of the exciton phenomenologically. However there is one point that we should take care of. The solution $\varrho(t)$ of the Liouville Eq. (1) must always satisfies the identity $\text{Tr}\varrho(t) = 1$. This condition seems very trivial, but popular methods to calculate nonlinear responses, *e.g.*, equation of motion, or optical Bloch equation, sometimes break this identity by introducing phenomenological damping effect, and give rise to unphysical divergences in the nonlinear susceptibility. (See also Ref. [24].) When we treat the random system, this normalization condition becomes more important, because we have to have physical quantities averaged over the random configuration.

In order to write down the matrix elements of $L_\gamma \varrho$, we first introduce formally the ground state $|g\rangle$, one-exciton eigenstates $|\alpha\rangle$, and two-exciton eigenstates $|(\sigma\sigma')\rangle$ of Hamiltonian H_0. Here the symbol $(\sigma\sigma')$ formally represents a state of two excitations. Because of the Pauli's exclusion principle, there are N one-exciton eigenstates and $N(N-1)/2$ two-exciton eigenstates. Then we designate the eigen energies of these states as

$$H_0|g\rangle = 0, \tag{7a}$$

$$H_0|\alpha\rangle = \Omega_\alpha|\alpha\rangle, \tag{7b}$$

$$H_0|(\sigma\sigma')\rangle = \Omega_{\sigma\sigma'}|(\sigma\sigma')\rangle. \tag{7c}$$

As is shown later, it suffices to consider only matrix elements involving one-exciton eigenstates and the ground state under resonant pumping of excitons. For completeness, however, we here assume rather general form for the Liouville operator $L_\gamma \varrho$ as follows:

$$\langle g | L_\gamma \varrho | g \rangle \equiv 2 \sum_\alpha \gamma_\alpha \varrho_{\alpha,\alpha} + 2 \sum_{(\sigma\sigma')} \gamma_{\sigma\sigma'} \varrho_{\sigma\sigma',\sigma\sigma'} , \tag{8a}$$

$$\langle \alpha | L_\gamma \varrho | g \rangle \equiv -\gamma_\alpha \varrho_{\alpha,g} , \tag{8b}$$

$$\langle \alpha | L_\gamma \varrho | \beta \rangle \equiv -(\gamma_\alpha + \gamma_\beta) \varrho_{\alpha,\beta} , \tag{8c}$$

$$\langle (\sigma\sigma') | L_\gamma \varrho | g \rangle \equiv -\gamma_{\sigma\sigma'} \varrho_{\sigma\sigma',g} , \tag{8d}$$

$$\langle (\sigma\sigma') | L_\gamma \varrho | \alpha \rangle \equiv -(\gamma_{\sigma\sigma'} + \gamma_\alpha) \varrho_{\sigma\sigma',\alpha} , \tag{8e}$$

$$\langle (\sigma_1\sigma_1') | L_\gamma \varrho | (\sigma_2\sigma_2') \rangle \equiv -(\gamma_{\sigma_1\sigma_1'} + \gamma_{\sigma_2\sigma_2'}) \varrho_{\sigma_1\sigma_1',\sigma_2\sigma_2'} . \tag{8f}$$

Here we designate the longitudinal relaxation of the one-exciton state $|\alpha\rangle$ by γ_α and that of the two-exciton state $|\sigma\sigma'\rangle$ by and $\gamma_{\sigma\sigma'}$. It can be easily confirmed that the relaxation matrix $L_\gamma \varrho$ introduced above conserves the probability. The solution $\varrho(t)$ of the Liouville Eq. (1) always satisfies the identity $\text{Tr}\varrho(t) = 1$, so that we come across no unphysical divergences in the nonlinear susceptibility arising from the lack of conservation of probability, as stated previously. In later chapters, we assume that the relaxation rates γ_α's are independent of the state, and much smaller than the pure dephasing rate γ' due to impurity, i.e., $\gamma_\alpha = \gamma \ll \gamma'$. It is noted that the effect of the pure dephasing processes is taken account of, not in the relaxation matrix $L_\gamma \varrho$, but in the Hamiltonian H_0. The pure dephasing rate γ' is evaluated by the Born approximation of impurity

scattering in Chapter 4.

2.3 Summary of our model

In this chapter, we have introduced the microscopic model which is suitable for linear and nonlinear responses in the disordered system. It should be emphasized that the dephasing process of an exciton is included in the Hamiltonian H_0, and we take full account of the effect of random on-site energies microscopically. As for the longitudinal relaxation of an exciton, we use a tractable and plausible form of the Liouville operator $L_\gamma \varrho$, which does not break the probability condition $\mathrm{Tr}\varrho = 1$. Thus there is no unphysical divergence in calculation of nonlinear responses even in the random system. In the next chapter, we will evaluate optical linear and nonlinear responses under a rotating wave approximation.

(a) $|g\rangle$

(b) $|i\rangle = S_i^\dagger|g\rangle$

(c) $|ij\rangle = S_i^\dagger S_j^\dagger|g\rangle$
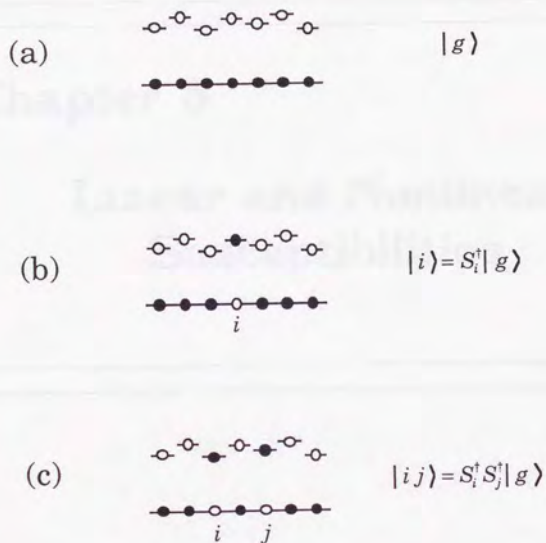
Figure 2.1

Schematic representation of the states of the Frenkel excitons with random onsite energies. (a): The ground state. (b): an instance of the one-exciton states. A pair of an electron and a hole is located at the site i. (c): an instance of the two-exciton states. Two pairs of an electron and a hole are located at the sites i and j ($i \neq j$).

Chapter 3

Linear and Nonlinear Susceptibilities

3.1 Expansion in the external electric field

In this chapter, we survey how linear and nonlinear optical polarizations and susceptibilities are evaluated. Throughout this chapter, we use a rotational wave approximation. Our interest is focused much upon the nearly degenerate four-wave mixing under resonant exciton pumping. However, the results obtained in this chapter is general under a rotational wave approximation.

The electronic polarization of the system is calculated through the solution $\varrho(t)$ by

$$\boldsymbol{P}(\boldsymbol{r},t) = \left\langle \mathrm{Tr}\left\{ \hat{\boldsymbol{P}}(\boldsymbol{r})\,\varrho(t) \right\} \right\rangle_{av}. \tag{1}$$

It is important that we take the ensemble average $\langle \cdots \rangle_{av}$ of the physical quantity over random configuration of onsite energies. We believe that this procedure is one of the most reliable one to evaluate the nonlinear polarization in the random system, because such methods as the equation-of-motion method may suffer from the ambiguity in the order of taking the quantum average and the random configuration average. To take account of the random distribution of energy levels averaging, we will evaluate Eq. (1) by resorting to the diagrammatic perturbation as to disorder effect in the next chapter. Linear and nonlinear polarizations are evaluated by expanding the density matrix $\varrho(t)$ in $H'(t)$ to the third-order. Liouville equation can be formally rewritten as

$$\frac{\partial}{\partial t}\varrho = \mathcal{L}_0\,\varrho + \mathcal{L}_1(t)\varrho, \tag{2}$$

where we introduce the Liouville operators $\mathcal{L}_0$ and $\mathcal{L}_1(t)$ by

$$\mathcal{L}_0 = -i\left[H_0,\cdot\right] + \mathcal{L}_\gamma, \tag{3a}$$

$$L_1(t) = -i[H'(t), \cdot \,]. \tag{3b}$$

To solve the density matrix $\varrho(t)$ in the expansion of $H'(t)$, we may well use the interaction picture as

$$\varrho(t) = e^{L_0 t}\, \tilde{\varrho}(t). \tag{4}$$

If we write down the relation between $\varrho(t)$ and $\tilde{\varrho}(t)$ given by Eq. (4) in the form of the matrix elements, it becomes as follows:

$$\varrho_{gg} = \tilde{\varrho}_{gg} + \sum_\alpha [1 - \exp(-2\gamma_\alpha t)]\tilde{\varrho}_{\alpha,\alpha} + \sum_{(\sigma\sigma')}[1 - \exp(-2\gamma_{\sigma\sigma'}t)]\tilde{\varrho}_{\sigma\sigma',\sigma\sigma'}, \tag{5a}$$

$$\varrho_{g,\alpha} = \exp[(-\gamma_\alpha + i\Omega_\alpha)t]\tilde{\varrho}_{g,\alpha}, \tag{5b}$$

$$\varrho_{\alpha,g} = \exp[(-\gamma_\alpha - i\Omega_\alpha)t]\tilde{\varrho}_{\alpha,g}, \tag{5c}$$

$$\varrho_{\alpha,\beta} = \exp[(-\gamma_\alpha - \gamma_\beta - i\Omega_\alpha + i\Omega_\beta)t]\tilde{\varrho}_{\alpha,\beta}, \tag{5d}$$

$$\varrho_{\sigma\sigma',g} = \exp[(-\gamma_{\sigma\sigma'} - i\Omega_{\sigma\sigma'})t]\tilde{\varrho}_{\sigma\sigma',g}, \tag{5e}$$

$$\varrho_{g,\sigma\sigma'} = \exp[(-\gamma_{\sigma\sigma'} + i\Omega_{\sigma\sigma'})t]\tilde{\varrho}_{g,\sigma\sigma'}, \tag{5f}$$

$$\varrho_{\sigma\sigma',\alpha} = \exp[(-\gamma_{\sigma\sigma'} - \gamma_\alpha - i\Omega_{\sigma\sigma'} + i\Omega_\alpha)t]\tilde{\varrho}_{\sigma\sigma',\alpha}, \tag{5g}$$

$$\varrho_{\alpha,\sigma\sigma'} = \exp[(-\gamma_\alpha - \gamma_{\sigma\sigma'} - i\Omega_\alpha + i\Omega_{\sigma\sigma'})t]\tilde{\varrho}_{\alpha,\sigma\sigma'}, \tag{5h}$$

$$\varrho_{\sigma\sigma',\sigma''\sigma'''} = \exp[(-\gamma_{\sigma\sigma'} - \gamma_{\sigma''\sigma'''} - i\Omega_{\sigma\sigma'} + i\Omega_{\sigma''\sigma'''})t]\tilde{\varrho}_{\sigma\sigma',\sigma''\sigma'''}. \tag{5i}$$

The density matrix in the interaction picture $\tilde{\varrho}(t)$ satisfies the Liouville equation

$$\frac{\partial}{\partial t}\tilde{\varrho} = \tilde{L}_1(t)\tilde{\varrho}, \tag{6}$$

where

$$\tilde{L}_1(t) \equiv e^{-L_0 t} L_1(t) e^{L_0 t}. \tag{7}$$

It is straightforward that we write down the Liouville equation in the interaction picture by the matrix elements;

$$\frac{\partial}{\partial t}\tilde{\varrho}_{g,\alpha} = (-i)e^{(\gamma_\alpha - i\Omega_\alpha)t}\left[\sum_\beta H'_{g,\beta}\varrho_{\beta,\alpha} - \varrho_{gg}H'_{g,\alpha} - \sum_{(\sigma\sigma')}\varrho_{g,\sigma\sigma'}H'_{\sigma\sigma',\alpha}\right], \tag{8a}$$

$$\frac{\partial}{\partial t}\tilde{\varrho}_{\alpha,g} = (-i)e^{(\gamma_\alpha + i\Omega_\alpha)t}\left[H'_{\alpha,g}\,\varrho_{gg} + \sum_{(\sigma\sigma')}H'_{\alpha,\sigma\sigma'}\,\varrho_{\sigma\sigma',g} - \sum_\beta \varrho_{\alpha,\beta}\,H'_{\beta,g}\right], \tag{8b}$$

$$\frac{\partial}{\partial t}\tilde{\varrho}_{\alpha,\beta} = (-i)e^{(\gamma_\alpha + \gamma_\beta + i\Omega_\alpha - i\Omega_\beta)t}$$

$$\times\left[H'_{\alpha,g}\,\varrho_{g,\beta} - \varrho_{\alpha,g}\,H'_{g,\beta} + \sum_{(\sigma\sigma')}\left(H'_{\alpha,\sigma\sigma'}\,\varrho_{\sigma\sigma',\beta} - \varrho_{\alpha,\sigma\sigma'}\,H'_{\sigma\sigma',\beta}\right)\right], \tag{9}$$

$$\frac{\partial}{\partial t}\tilde{\varrho}_{\sigma\sigma',g} = (-i)e^{(\gamma_{\sigma\sigma'} + i\Omega_{\sigma\sigma'})t}\sum_\alpha\left(H'_{\sigma\sigma',\alpha}\,\varrho_{\alpha,g} - \varrho_{\sigma\sigma',\alpha}\,H'_{\alpha,g}\right), \tag{10a}$$

$$\frac{\partial}{\partial t}\tilde{\varrho}_{g,\sigma\sigma'} = (-i)e^{(\gamma_{\sigma\sigma'} - i\Omega_{\sigma\sigma'})t}\sum_\alpha\left(H'_{g,\alpha}\varrho_{\alpha,\sigma\sigma'} - \varrho_{g,\alpha}H'_{\alpha,\sigma\sigma'}\right), \tag{10b}$$

$$\frac{\partial}{\partial t}\tilde{\varrho}_{\sigma\sigma',\alpha} = (-i)e^{(\gamma_{\sigma\sigma'} + \gamma_\alpha + i\Omega_{\sigma\sigma'} - i\Omega_\alpha)t}\left[\sum_\beta H'_{\sigma\sigma',\beta}\,\varrho_{\beta,\alpha} - \sum_{(\sigma''\sigma''')}\varrho_{\sigma\sigma',\sigma''\sigma'''}H'_{\sigma''\sigma''',\alpha} - \varrho_{\sigma\sigma',g}H'_{g,\alpha}\right], \tag{11a}$$

$$\frac{\partial}{\partial t}\tilde{\varrho}_{\alpha,\sigma\sigma'} = (-i)e^{(\gamma_\alpha + \gamma_{\sigma\sigma'} + i\Omega_\alpha - i\Omega_{\sigma\sigma'})t}\left[H'_{\alpha g}\,\varrho_{g,\sigma\sigma'} + \sum_{(\sigma''\sigma''')}H'_{\alpha,\sigma''\sigma'''}\,\varrho_{\sigma''\sigma''',\sigma\sigma'} - \sum_\beta \varrho_{\alpha,\beta}H'_{\beta,\sigma\sigma'}\right], \tag{11b}$$

$$\frac{\partial}{\partial t}\tilde{\varrho}_{\sigma\sigma',\sigma''\sigma'''} = (-i)e^{(\gamma_{\sigma\sigma'} + \gamma_{\sigma''\sigma'''} + i\Omega_{\sigma\sigma'} - i\Omega_{\sigma''\sigma'''})t}\sum_\alpha\left(H'_{\sigma\sigma',\alpha}\,\varrho_{\alpha,\sigma''\sigma'''} - \varrho_{\sigma\sigma',\alpha}\,H'_{\alpha,\sigma''\sigma'''}\right). \tag{12}$$

The formal solution of Eq. (2) is given by

$$\varrho(t) = \mathcal{U}(t,-\infty)\,\varrho(-\infty), \tag{11}$$

where the operator $\mathcal{U}$ in the Liouville space can be expressed with the time-ordered exponential as

$$\mathcal{U}(t,t') = e^{\mathcal{L}_0 t}\,T\exp\left[\int_{t'}^t \tilde{\mathcal{L}}_1(t_1)dt_1\right]e^{-\mathcal{L}_0 t'}. \tag{12}$$

At time $t \to -\infty$, we assume the electronic system to be at the ground state: $\varrho(-\infty) = \varrho_0 \equiv |g\rangle\langle g|$. The interaction $H'(t)$ is adiabatically switched on. By expanding the time-ordered exponential, we obtain the density matrix expanded in a perturbation series of $H'(t)$:

$$\varrho(t) = \varrho^{(0)}(t) + \varrho^{(1)}(t) + \varrho^{(2)}(t) + \varrho^{(3)}(t) + \cdots, \tag{13}$$

where

$$\varrho^{(0)}(t) = \varrho_0, \tag{14a}$$

$$\varrho^{(1)}(t) = e^{\mathcal{L}_0 t} \int_{-\infty}^{t} dt_1 \tilde{\mathcal{L}}_1(t_1)\, \varrho_0, \tag{14b}$$

$$\varrho^{(2)}(t) = e^{\mathcal{L}_0 t} \int_{-\infty}^{t} dt_2 \int_{-\infty}^{t_2} dt_1 \tilde{\mathcal{L}}_1(t_2)\tilde{\mathcal{L}}_1(t_1)\, \varrho_0, \tag{14c}$$

$$\varrho^{(3)}(t) = e^{\mathcal{L}_0 t} \int_{-\infty}^{t} dt_3 \int_{-\infty}^{t_3} dt_2 \int_{-\infty}^{t_2} dt_1 \tilde{\mathcal{L}}_1(t_3)\tilde{\mathcal{L}}_1(t_2)\tilde{\mathcal{L}}_1(t_1)\, \varrho_0. \tag{14d}$$

Linear and nonlinear polarizations (and susceptibilities also) are defined using the density matrices $\varrho^{(1)}(t)$ and $\varrho^{(3)}(t)$ as

$$\boldsymbol{P}^{(1)}(\boldsymbol{r},t) = \left\langle \mathrm{Tr}\left\{ \hat{\boldsymbol{P}}(\boldsymbol{r})\, \varrho^{(1)}(t) \right\} \right\rangle_{av}, \tag{15a}$$

$$\boldsymbol{P}^{(3)}(\boldsymbol{r},t) = \left\langle \mathrm{Tr}\left\{ \hat{\boldsymbol{P}}(\boldsymbol{r})\, \varrho^{(3)}(t) \right\} \right\rangle_{av}. \tag{15b}$$

The second-order nonlinear polarization $\boldsymbol{P}^{(2)}(\boldsymbol{r},t)$ is found to vanish. In the following calculation, we use a rotational wave approximation to evaluate linear and nonlinear susceptibilities.

3.2 Linear Susceptibility

We define the linear susceptibility by

$$\boldsymbol{P}^{(1)}(\boldsymbol{r},t) = -\frac{N}{V}\sum_{\boldsymbol{k}_l}\sum_{l=1}^{3} \chi^{(1)} : \boldsymbol{E}_l e^{i\boldsymbol{k}_l \cdot \boldsymbol{r} - i\omega_l t} + (\text{c.c.}). \tag{16}$$

The evaluation is straightforward through Eqs. (14b) and (15a). Under a rotating wave approximation, we obtain a stationary solution as

$$\varrho_{\alpha,g}^{(1)}(t) = -\sum_l \frac{\sqrt{N}\boldsymbol{\mu}\langle\alpha|\boldsymbol{k}_l\rangle\, \boldsymbol{E}_l e^{-i\omega_l t}}{\omega_l - \Omega_\alpha + i\gamma_\alpha}. \tag{17}$$

Therefore linear susceptibility $\chi^{(1)}$ is given by

$$\chi^{(1)} = \left\langle \sum_\alpha \frac{\mu\mu \langle k_s | \alpha \rangle \langle \alpha | k_l \rangle}{\omega_l - \Omega_\alpha + i\gamma_\alpha} \right\rangle_{av}.$$ (18)

The disorder effect on the linear susceptibility is included fully in the one-state eigen energies Ω_α and the random configuration averaging $\langle \cdots \rangle_{av}$. It will be evaluated by the perturbational calculation in the next chapter.

3.3 Third-order Nonlinear Susceptibility

Since the second-order nonlinear susceptibility will vanish, we go on to the calculation of the third-order nonlinear susceptibility. The third-order nonlinear susceptibility is defined by

$$\boldsymbol{P}^{(3)}(\boldsymbol{r},t) = \sum_{k_s} \sum_{l,m,n=1}^{3} \chi^{(3)} : E_l E_m^* E_n e^{i k_s \cdot r - i \omega_s t} + (\text{c.c.}),$$ (19)

where $(\omega_s, \boldsymbol{k}_s) = (\omega_l - \omega_m + \omega_n, \boldsymbol{k}_l - \boldsymbol{k}_m + \boldsymbol{k}_n)$. As will be given in Appendix A, the dimension of $\chi^{(3)}$ is $[E^{-1}][L^d]$. (Here $[E]$ and $[L]$ are, respectively, the dimensions of the energy and the length.) Evaluation of $\chi^{(3)}$ under a rotational wave approximation is done through Eqs. (14d) and (15b) after some calculation. The result is summarized by help of the double Feynman diagrams (see, *e.g.* Ref. [25]) of Fig. 3.1 as

$$\chi^{(3)} = \chi^{(3)}_{1+2} + \chi^{(3)}_{3+4} + \chi^{(3)}_5 + \chi^{(3)}_{6+7} + \chi^{(3)}_8.$$ (20)

The third-order susceptibility $\chi^{(3)}$ consists of five terms from eight diagrams depicted in Fig. 3.1: each suffix of $\chi^{(3)}_i$ denotes the contribution from i-th diagram in the figure. Detailed form of each term is given as follows :

$$\chi^{(3)}_{1+2} = \frac{N^2}{V} \left\langle \sum_{\alpha,\beta} \frac{\mu\mu\mu\mu \, \langle k_s | \alpha \rangle \langle \alpha | k_n \rangle \langle k_m | \beta \rangle \langle \beta | k_l \rangle}{(\omega_s - \Omega_\alpha + i\gamma_\alpha)(\omega_l - \Omega_\beta + i\gamma_\beta)(\omega_m - \Omega_\beta - i\gamma_\beta)} \right\rangle_{av},$$ (21a)

$$\chi_{3+4}^{(3)} = \frac{N^2}{V}\left\langle \sum_{\alpha,\beta} \frac{\mu\mu\mu\mu \ \langle k_s|\alpha\rangle\langle\alpha|k_n\rangle\langle k_m|\beta\rangle\langle\beta|k_l\rangle}{(\omega_s - \Omega_\alpha + i\gamma_\alpha)(\omega_n - \Omega_\alpha + i\gamma_\alpha)(\omega_m - \Omega_\beta - i\gamma_\beta)}\right\rangle_{av}, \tag{21b}$$

$$\chi_5^{(3)} = -\frac{N^2}{V}\left\langle \sum_{\alpha,\beta,(\sigma\sigma')} \frac{\mu\mu\mu\mu \ \langle k_s|\alpha\rangle\langle\alpha k_m|(\sigma\sigma')\rangle\langle(\sigma\sigma')|\beta k_n\rangle\langle\beta|k_l\rangle}{(\omega_s - \Omega_\alpha + i\gamma_\alpha)(\omega_l + \omega_n - \Omega_{\sigma\sigma'} + i\gamma_{\sigma\sigma'})(\omega_l - \Omega_\beta + i\gamma_\beta)}\right\rangle_{av}, \tag{21c}$$

$$\chi_{6+7}^{(3)} = -\frac{N^2}{V}\left\langle \sum_{\alpha,\beta,(\sigma\sigma')} \frac{\mu\mu\mu\mu \ \langle k_m|\alpha\rangle\langle\alpha k_s|(\sigma\sigma')\rangle\langle(\sigma\sigma')|\beta k_n\rangle\langle\beta|k_l\rangle}{(\omega_s + \Omega_\alpha - \Omega_{\sigma\sigma'} + i\gamma_\alpha + i\gamma_{\sigma\sigma'})(\omega_l - \Omega_\alpha + i\gamma_\alpha)(\omega_m - \Omega_\beta - i\gamma_\beta)}\right\rangle_{av},$$

$$\tag{21d}$$

$$\chi_8^{(3)} = \frac{N^2}{V} \sum_{\alpha,\beta,(\sigma\sigma')}\left\langle \frac{\mu\mu\mu\mu \ \langle k_m|\alpha\rangle\langle\alpha k_s|(\sigma\sigma')\rangle\langle(\sigma\sigma')|\beta k_n\rangle\langle\beta|k_l\rangle}{(\omega_s + \Omega_\alpha - \Omega_{\sigma\sigma'} + i\gamma_\alpha + i\gamma_{\sigma\sigma'})(\omega_l + \omega_n - \Omega_{\sigma\sigma'} + i\gamma_{\sigma\sigma'})(\omega_l - \Omega_\beta + i\gamma_\beta)}\right\rangle_{av}.$$

$$\tag{21e}$$

Here we use the notation of $|k\rangle \equiv \sum_i \langle i|k\rangle S_i^+|g\rangle$ and $|\beta k\rangle \equiv S_\beta^+|k\rangle = \sum_\beta \langle i|\beta\rangle S_i^+|k\rangle$. The third-order optical susceptibility should be proportional to atomic density N/V for the bulk material. It should be emphasized that the expressions obtained above include all the effects due to disorder and finite sample size. What is difficult lies in obtaining the eigenstates of the Hamiltonian H_0 and in taking the ensemble average over random impurity configuration. In the following chapter, we show that such difficulty will be overcome under resonant pumping of excitons[*]. We will find the factor N^2/V in the expression of $\chi^{(3)}$ to be reduced naturally to $(N/V)N_{\text{eff}}$, where N_{eff} is the enhancement factor of the nonlinear optical polarization we will define.

---

[*] It is because the leading contribution to the nonlinear susceptibility as to the expansion in γ/γ' is given by $\chi_{1+2}^{(3)} + \chi_{3+4}^{(3)}$, which can be estimated through the knowledge of the one-exciton states only. It will be given in Chapter 4.
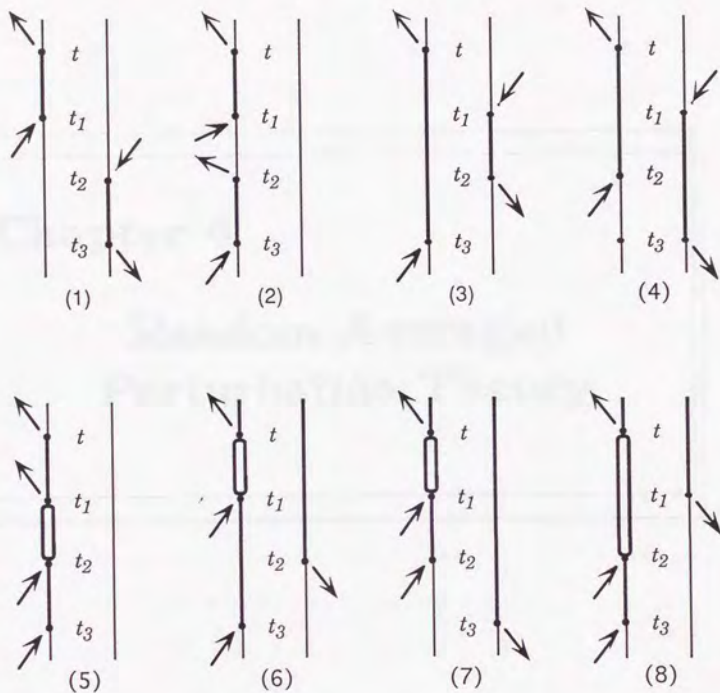
Figure 3.1

All the processes contributing to the third-order nonlinear polarization under rotating wave approximation in the double Feynman diagrams. Thick lines and double thick lines denote one-exciton and two-exciton states, respectively. The diagrams (1) – (4) give dominant contribution to the third-order polarization under resonant pumping.

Chapter 4

Random Averaged Perturbation Theory

4.1 Introduction to Random Averaged Perturbation Theory

In this chapter, we examine the disorder effect both on the linear and nonlinear susceptibilities by the perturbational expansion from the delocalized limit. To justify this expansion, W/T must be small. Based upon the expressions obtained in the previous chapter, we evaluate $\chi^{(1)}$ and $\chi^{(3)}$ by help of diagrams. Our concern will be focused upon the optical nonlinear susceptibility in the random system. We will establish the relation between the third-order nonlinear polarization and the exciton's diffusive propagation, and the peculiarity of the phase-conjugation in the random system will be clarified.

In investigating the exciton propagation in the disordered medium, two diffusion modes are relevant: the particle-hole mode (diffuson) and the particle-particle mode (cooperon) [23]. They are depicted in Fig. 4.1. Whereas the diffuson mode corresponds to the forward coherent scattering process, the cooperon mode describes that the backward scattering amplitude is enhanced by multiple impurity scatterings, as a result of constructive interference between two processes that are connected with each other by time-reversal symmetry. Since the phase conjugation is a process generating a wave whose phase is complex conjugate to the incident probe wave, it is very natural that nonlinear polarization for the phase conjugation is expressed by use of the cooperon mode [9–14]. When the incident waves are under resonant pumping of the exciton, we will find that the enhancement factor N_{eff} for the phase-conjugated signal is directly written down by the cooperon mode with the momentum and the frequency specified by the external electric field.

We first evaluate the linear susceptibility in Sec. 4.1. It will be found that

the onsite random energies give the dephasing relaxation rate to the linear susceptibility $\chi^{(1)}$. In Sec. 4.2 and later, we will examine the disorder effect on the nonlinear susceptibility. We will define the enhancement factor N_{eff} of the nonlinear susceptibility, and find that N_{eff} is closely related to the cooperon mode in the case of the phase-conjugated wave generation.

In the following treatment, we neglect the state dependence of the rate of decay into the ground state. Thus set all γ_α's to a constant γ. As we said in Sec. 2.1, we assume the situation that γ is much smaller than the dephasing rate coming from random onsite energies[*]. In addition, we assume all the external radiation fields have the same polarization, and designate the parallel component of the atomic transition dipolemoment μ as μ. For the sake of convenience, we introduce the retarded and advanced Green functions by

$$\hat{G}^{R,A}(z) = \left[z - H_0 \pm i\gamma\right]^{-1}. \tag{1}$$

It is noted that the Green functions of Eq. (1) are not c-numbers but operators.

4.2 Disorder Effect on Linear Susceptibility

To begin with, we examine the disorder effect on linear susceptibility $\chi^{(1)}$. The linear susceptibility is given by (18) in Chapter 3, and can be expressed in terms of the Green function introduced above as follows:

$$\chi^{(1)} = \mu^2 \left\langle \left\langle \boldsymbol{k}_s \left| \hat{G}^R(\omega_l) \right| \boldsymbol{k}_l \right\rangle \right\rangle_{av}. \tag{2}$$

Thus evaluating linear susceptibility is reduced to that of the averaged retarded

---

[*] The dephasing rate due to random onsite energies will be designated by γ' later.

one-particle Green functions $G_{k_s}^{R,A}(\omega_l)$, which is defined by

$$\left\langle\left\langle \boldsymbol{k}_s \middle| \hat{G}^{R,A}(\omega) \middle| \boldsymbol{k}_l \right\rangle\right\rangle_{av} = G_{k_s}^{R,A}(\omega)\,\delta_{\boldsymbol{k}_s,\boldsymbol{k}_l}. \tag{3}$$

To evaluate $G_{k_s}^{R,A}(\omega)$, we introduce the self-energy of the exciton $\Sigma_k^{R,A}(\omega)$ by

$$G_k^{R,A}(\omega) = \frac{1}{(\omega - \Omega_k \pm i\gamma) - \Sigma_k^{R,A}(\omega)}. \tag{4}$$

The symbol Ω_k denotes the exciton's dispersion relation in the system without disorder. The self-energy $\Sigma_k^{R,A}(\omega)$ is evaluated in the Born approximation as in Fig. 4.2. The imaginary part of the self-energy part $\Sigma_k^{R,A}(\omega)$ will define the pure dephasing rate γ'. The real part of $\Sigma_k^{R,A}(\omega)$ means an energy shift. Disorder-induced redshift relative to the homogeneous spectrum is known well [26,27], but it is not our present purpose to go into the detail of it. Neglecting the real part of the self-energy $\Sigma_k^{R,A}(\omega)$, we obtain:

$$\Sigma_k^{R,A}(\omega) = \frac{W^2}{N}\sum_i \left\langle i \middle| \hat{G}^{R,A}(\omega) \middle| i \right\rangle = \mp i\pi N_0 W^2\left(\tfrac{V}{N}\right) = \mp i\gamma', \tag{5}$$

where N_0 is the average state density of the exciton per unit volume and unit energy at frequency ω_0. Thus the averaged retarded and advanced Green function are expressed by

$$G_k^{R,A}(\omega) = \left[\omega - \Omega_k \pm i(\gamma + \gamma')\right]^{-1}. \tag{6}$$

Hence linear susceptibility is evaluated as

$$\chi^{(1)} = \frac{\mu^2}{\omega_l - \Omega_{k_l} + i(\gamma' + \gamma)}. \tag{7}$$

We find that the disorder effect on linear susceptibility merely gives the pure-dephasing rate due to scattering by impurities, as is expected. No singular behavior of linear susceptibility is anticipated even around the exciton mobility edge. However if we go on to the evaluation of the nonlinear susceptibility,

disorder in the system will be found to give quite a different effect. This will be given in the next section.

4.3 Disorder Effect on Phase-Conjugated Wave Generation

4.3.1 Nonlinear Susceptibility in resonant region

Now we will examine the third-order nonlinear susceptibility defined by

$$P^{(3)}(r,t) = \sum_{k_s} \sum_{l,m,n=1}^{3} \chi^{(3)} : E_l E_m^* E_n e^{ik_s \cdot r - i\omega_s t} + \text{(c.c.)}, \tag{8}$$

where $(\omega_s, k_s) = (\omega_l - \omega_m + \omega_n, k_l - k_m + k_n)$. The explicit expression of $\chi^{(3)}$ was obtained in the previous chapter. The result was given by Eqs. (20) and (21a)–(21e) in Chapter 3. The experimental geometry was illustrated in Fig. 1.2. If we use a rotational wave approximation, three kinds of signal waves can be observed, depending upon the combinational order of frequencies and momenta as in Fig. 4.3 and in Table 4.4. The phase-conjugated signal $(\omega_s, k_s) = (2\omega_0 - \omega_p, k_f + k_b - k_p)$ is observed in the cases $(l, m, n) = (f, p, b)$ and (b, p, f).

As is stated previously, the pure dephasing rate γ' given by Eq. (5) is assumed to be much larger than γ. We retain the leading terms by expanding Eq. (20) of Chapter 3 in $\gamma/\gamma' (\ll 1)$ under nearly resonant pumping of excitons. In resonant region, the dominant contribution coming from the diagrams (1)–(4) of Fig. 3.1 is found to be larger by the order of magnitude $\gamma'/\gamma (\gg 1)$ than that from (5)–(8). It is because the former terms have exactly the same eigen energy in the denominator and thus these terms have the factor γ in the denominator at the phase-conjugated wave generation. The latter ones don't have the same eigen energies in the denominator, so will have the factor of the order $\gamma + \gamma'$ in

the denominator. (See also Ref. [28]). Therefore the dominant contribution to the third-order optical polarization producing phase-conjugated waves in resonant region is given by

$$\chi^{(3)} \cong \chi^{(3)}_{1+2} + \chi^{(3)}_{3+4} \ . \tag{9}$$

Recently the third-order nonlinear susceptibility of disordered aggregates is investigated in Ref. [29–31]. Since the one-dimensional XXZ model can be transformed into the fermion model by use of the Jordan-Wigner transformation, the eigenstates of the disordered aggregates are found to be fermion states [32]. In Ref. [31], the exact result by the Jordan-Wigner transformation is compared with the result obtained by the local field approximation or that by what he called the "excitonic two-level system" approximation which is identical to Eq. (9). He concluded as follows: (1) Whereas the local field approximation correctly describes the nonresonant nonlinear response, it cannot describe the on-resonant nonlinear absorption. (2) By contrast, the approximation given by Eq. (9) may very well describe the on-resonant nonlinear response and it rapidly improves for growing disorder, though it does not recover the exact off-resonant behavior.

We will show the dominant contribution to the third-order susceptibility given by Eq. (9) shows a singular behavior as a function of the detuning frequency $\delta\omega \equiv \omega_s - \omega_p$ and the misalignment between the forward and backward pump beams, $\boldsymbol{q} \equiv \boldsymbol{k}_f + \boldsymbol{k}_b$, when both are around zero.

4.3.2 The Enhancement Factor and the Coherent Volume function

We define the enhancement factor N_{eff}, which measures how many atoms

(or molecules) can contribute coherently to the nonlinear optical polarization. The enhancement factor N_{eff} for the phase-conjugated wave generation is introduced as follows:

$$\chi^{(3)} = N_{\text{eff}} \left(\tfrac{N}{V}\right) \frac{\mu^4}{(2i\gamma)} G_{k_s}^R(\omega_s) G_{k_p}^A(\omega_p). \tag{10}$$

To get the microscopic expression of the enhancement factor N_{eff}, we rewrite Eqs. (21a) and (21b) of Chapter 3 in terms of the retarded and advanced Green functions introduced in Eq. (1). It leads to

$$\chi_{1+2}^{(3)} = \frac{N^2 \mu^4}{V} \left\langle \langle k_s | \hat{G}^R(\omega_s) | k_n \rangle \langle k_m | \hat{G}^R(\omega_l) \hat{G}^A(\omega_m) | k_l \rangle \right\rangle_{av}, \tag{11a}$$

$$\chi_{3+4}^{(3)} = \frac{N^2 \mu^4}{V} \left\langle \langle k_s | \hat{G}^R(\omega_s) \hat{G}^R(\omega_n) | k_n \rangle \langle k_m | \hat{G}^A(\omega_m) | k_l \rangle \right\rangle_{av}. \tag{11b}$$

Next we make use of the operator identities

$$\hat{G}^R(\omega_1) \hat{G}^A(\omega_2) = \frac{\hat{G}^A(\omega_2) - \hat{G}^R(\omega_1)}{\omega_1 - \omega_2 + 2i\gamma}, \tag{12a}$$

$$\hat{G}^R(\omega_1) \hat{G}^R(\omega_2) = \frac{\hat{G}^R(\omega_2) - \hat{G}^R(\omega_1)}{\omega_1 - \omega_2}. \tag{12b}$$

This identity allows us to transform the terms $\chi_{1+2}^{(3)}$ and $\chi_{3+4}^{(3)}$ into the summation of the averaged two-body Green functions. The evaluation of the averaged two-body Green functions is performed diagrammatically by decomposing them into the form of the vertex part and the averaged one-body Green functions. As stated previously, we take only the terms whose behavior becomes singular in the generation of phase-conjugated waves at $k_f + k_b \approx 0$ and $\omega_s - \omega_p \approx 0$ in evaluating the optical nonlinear susceptibility $\chi^{(3)}$. Other terms that will be neglected here give the contribution of the order $(\xi_{\text{coh}})^d N/V$ to N_{eff}, where $\xi_{\text{coh}} = [N_0(\gamma + \gamma')]^{-1/d}$ is the conventional coherent length of the exciton. This contribution is smaller by the order of magnitude $\gamma/\gamma' (\ll 1)$ than that we retain here. Hence we get

$$\chi_{1+2}^{(3)} \approx \frac{N^2 \mu^4 \left(G_{k_s}^R G_{k_b}^R G_{k_f}^A G_{k_p}^A \right)}{V} \cdot \frac{\Gamma(\omega_s - \omega_p)}{\omega_0 - \omega_p + 2i\gamma} + (f \leftrightarrow b), \tag{13a}$$

$$\chi_{3+4}^{(3)} \approx \frac{N^2 \mu^4 \left(G_{k_s}^R G_{k_b}^R G_{k_f}^A G_{k_p}^A \right)}{V} \cdot \frac{\Gamma(\omega_0 - \omega_p) - \Gamma(\omega_s - \omega_p)}{\omega_0 - \omega_s} + (f \leftrightarrow b). \tag{13b}$$

Here the vertex part $\Gamma(\omega_s - \omega_p)$, which is now constructed between the retarded and the advanced Green functions, depends also on the momenta of the three incident beams: k_f, k_b, and k_p, as illustrated in Fig. 4.5. The microscopic expression of the enhancement factor N_{eff} for phase-conjugated wave generation is obtained by comparison between the equations above and Eq. (10). We finally obtain the following result:

$$N_{eff} = \left(\tfrac{N}{V} \right) \left[1 - 2i\gamma \frac{\partial}{\partial \delta\omega} \right] \Xi(\delta\omega) \Big|_{\omega_s - \omega_p} + (f \leftrightarrow b), \tag{14}$$

$$\Xi(\omega_s - \omega_p) = G_{k_b}^R(\omega_s) G_{k_f}^A(\omega_p) \Gamma(\omega_s - \omega_p). \tag{15}$$

We will call the function Ξ the coherent volume function hereafter. As will be shown in the next chapter, the coherent function Ξ will play a central role in the renormalization of disorder effect. This is because $\chi^{(3)}$ has the dimension of $[L^d]$, as will be shown in Appendix A.

The vertex part $\Gamma(\omega_s - \omega_p)$ can be easily evaluated by the perturbational expansion from the delocalized limit, as is done in Ref. [9]. At the lowest order, the diffusion mode called cooperon (Fig. 4.1; see also Ref. [23]) is found to give the leading contribution at $q = k_f + k_b \approx 0$, and $\delta\omega = \omega_s - \omega_p \approx 0$ [9,11]. The cooperon mode depends only on $\delta\omega = \omega_s - \omega_p$ and $q = k_f + k_b$ like

$$\Gamma_c^{(0)}(\delta\omega; q) = \frac{\gamma'}{\pi N_0} \frac{2\gamma'}{D_0 q^2 - i\delta\omega + 2\gamma'}, \tag{16}$$

where $D_0 \equiv v_0^2 / 2d\gamma'$ is the bare diffusion coefficient and v_0 is the group velocity of the exciton. Corresponding to Eq. (16), we obtain the lowest order expression

of the coherent volume function $\Xi(\delta\omega)$ under nearly resonant exciton pumping as a function of $\delta\omega$ and q:

$$\Xi^{(0)}(\delta\omega;\boldsymbol{q}) \equiv \frac{2}{\pi} \frac{1}{N_0 D_0 q^2 + N_0(-i\delta\omega + 2\gamma)}. \tag{17}$$

The result shows that the coherent volume function for the completely phase-conjugated signal, *i.e.*, $\delta\omega = 0$ and $\boldsymbol{q} = \boldsymbol{0}$ in Eq. (17), is dominated by 2γ not by $\gamma + \gamma'$ in the delocalized limit.

4.3.3 Physical Explanation of the Result

The result obtained in the previous section can be easily understood by help of a Bergmann's figure of Fig. 4.6 [33]. Figure 4.6 illustrates how the incident probe $\boldsymbol{k}$ is scattered into $-\boldsymbol{k} + \boldsymbol{q}$ (phase-conjugated signal) via scattering sequences. First take the case generating a exactly phase-conjugated wave, *i.e.*, $\boldsymbol{q} = \boldsymbol{0}$. In the scattering process from the state $\boldsymbol{k}$ into $-\boldsymbol{k}$, there are complementary scattering series, one pair of which is illustrated in Fig. 4.5. They are the sequences

$$\boldsymbol{k} \rightarrow \boldsymbol{k}'_1 \rightarrow \boldsymbol{k}'_2 \rightarrow \boldsymbol{k}'_3 \rightarrow \boldsymbol{k}'_4 = -\boldsymbol{k} \tag{18a}$$

where the momentum transfers $\boldsymbol{g}_1, \boldsymbol{g}_2, \boldsymbol{g}_3, \boldsymbol{g}_4$ (along the upper semicircle), and

$$\boldsymbol{k} \rightarrow \boldsymbol{k}''_1 \rightarrow \boldsymbol{k}''_2 \rightarrow \boldsymbol{k}''_3 \rightarrow \boldsymbol{k}''_4 = -\boldsymbol{k} \tag{18b}$$

with the momentum transfers $\boldsymbol{g}_4, \boldsymbol{g}_3, \boldsymbol{g}_2, \boldsymbol{g}_1$ (along the lower semicircle). These two processes are time-reversal with each other, so that they have the same phase shift from random potentials. Thus their transition probabilities are identical to each other. Since the final amplitudes A' and A'' are equal, say, to A, the total intensity

$$\left|A' + A''\right|^2 = \left|A'\right|^2 + \left|A''\right|^2 + (A')^* A'' + A'(A'')^* \tag{19}$$

becomes $4\left|A\right|^2$. The backscattering intensity is two times as large as it would be if their phases were completely random, which is illustrated in Fig. 4.5(a). The finite momentum deviation q reduces this coherence of these scattering processes as in Fig. 4.6(b). In this case, the phase shift given from random potential can no longer be identical between the time reversal processes. It should be emphasized that disorder in the system gives both the positive and negative effects for getting large nonlinear optical responses, as we have already seen in this section and also in Sec. 1.3.

4.4 Summary of the Perturbational Calculation

In this chapter, we have presented the perturbational calculation of the linear and nonlinear susceptibility by the expansion in randomness. In Sec. 4.2, we have seen that randomness gives rise to the dephasing relaxation rate γ'. In Sec. 4.3, we have investigated the disorder effect on the nonlinear susceptibility. We have derived the microscopic expression of the enhancement factor of the nonlinear susceptibility, and clarified the peculiarity of the phase-conjugated wave generation in the random system. In particular, the enhancement factor for the phase-conjugated wave generation is found to be closely related to the diffusion mode called cooperon. In other words, we have shown within the lowest order perturbation theory that the observation of the phase-conjugated wave generation is equivalent to that of the diffusion mode (*i.e.*, the cooperon mode) with frequencies and momenta specified by the external electric field. In addition, we have given a physical picture by use of the Bergmann's figure about

the origin of the enhancement for the phase-conjugated wave generation. All the results obtained in this chapter is evaluated at the lowest order calculation. If disorder in the system increases, the localized-delocalized transition will occur. In the next chapter, we will investigate the behavior of the nonlinear susceptibility around the exciton mobility edge by constructing the scaling theory.

$$\Gamma_d^{(0)} = \quad + \quad + \quad + \cdots$$

(a)

$$\Gamma_c^{(0)} = \quad + \quad + \quad + \cdots$$

$$= \quad + \quad + \quad + \cdots$$

(b)
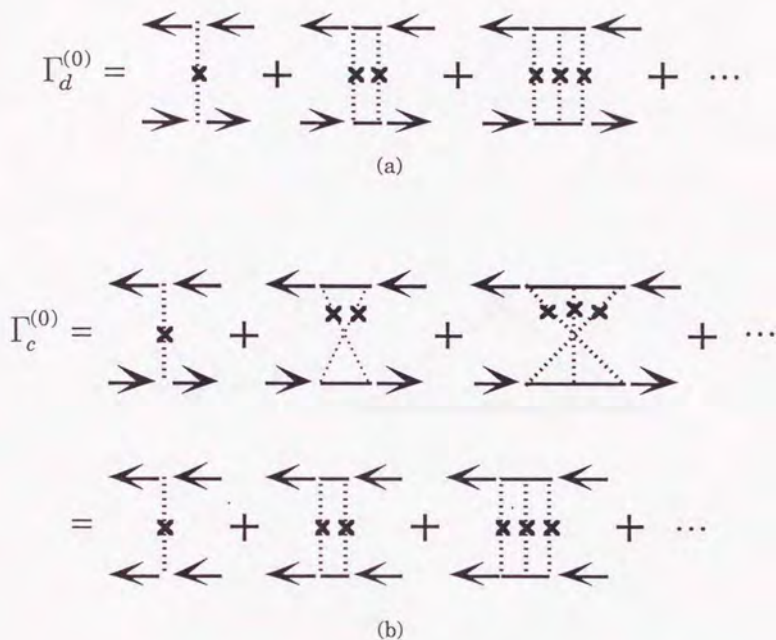
Figure 4.1

The two diffusion modes in the random system. Dash lines denote scattering of the exciton by the random onsite potential denoted by the cross. Upper arrows and lower arrows means, respectively, the retarded and advanced Green functions. These two modes will be found to give dominant contributions to $\chi^{(3)}$ at $q \equiv k_f + k_b \approx 0$. (See also Fig. 4.5.) (a): The ladder vertex part corresponds to the lowest-order *"diffuson"* mode (the particle-hole channel). (b): The maximally-crossed vertex part corresponds to the lowest-order *"cooperon"* mode (the particle-particle channel). If the direction of the advanced Green functions is reversed, the maximally-crossed vertex part is transformed to the ladder vertex part.

$$\Sigma_k(\omega) =$$

Figure 4.2

The self-energy of the averaged one-particle Green function. Dash lines denote scatterings of the exciton by the random onsite potential denoted by the cross. The random average is taken over the impurity position.
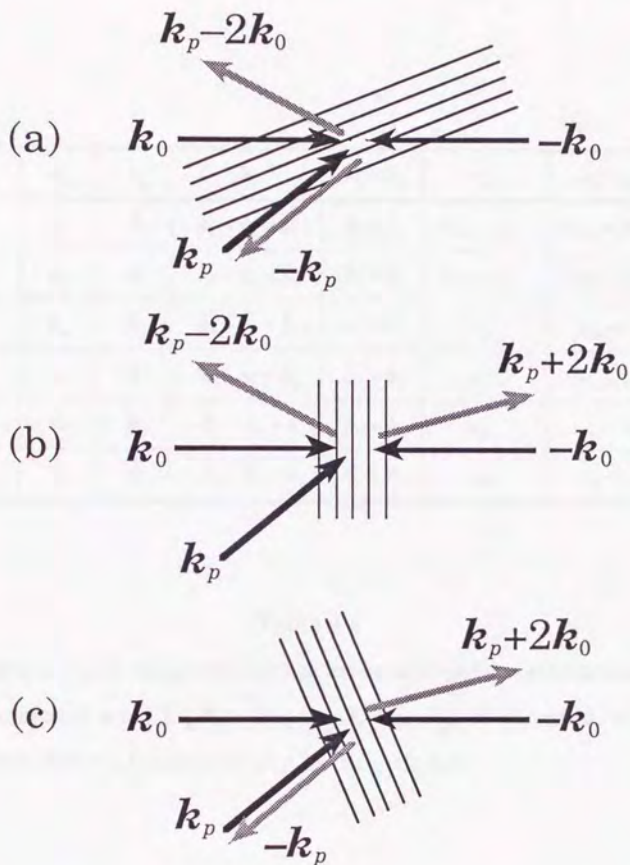
Figure 4.3

Three kinds of signal waves are observed through the reflection of the third wave by the three kinds of population gratings. The figure is illustrated for the case that the forward and backward pumping waves are applied exactly in the opposite direction, *i.e.*, $\boldsymbol{k}_f = \boldsymbol{k}_0$ and $\boldsymbol{k}_b = -\boldsymbol{k}_0$. (a): Population grating by $(\boldsymbol{k}_f, \omega_0)$ and $(\boldsymbol{k}_p, \omega_p)$. (b): Population grating by $(\boldsymbol{k}_f, \omega_0)$ and $(\boldsymbol{k}_b, \omega_0)$. (c): Population grating by $(\boldsymbol{k}_b, \omega_0)$ and $(\boldsymbol{k}_p, \omega_p)$.

k_l	k_m	k_n	k_s	$k_l + k_n$	ω_s	$\omega_s - \omega_m$
k_f	k_p	k_b	$k_f + k_b - k_p$	$k_f + k_b$	$2\omega_0 - \omega_p$	$2\omega_0 - 2\omega_p$
k_b	k_p	k_f	$k_f + k_b - k_p$	$k_f + k_b$	$2\omega_0 - \omega_p$	$2\omega_0 - 2\omega_p$
k_f	k_b	k_p	$k_f - k_b + k_p$	$k_f + k_p$	ω_p	$\omega_p - \omega_0$
k_p	k_b	k_f	$k_f - k_b + k_p$	$k_f + k_p$	ω_p	$\omega_p - \omega_0$
k_b	k_f	k_p	$-k_f + k_b + k_p$	$k_f + k_b$	ω_p	$\omega_p - \omega_0$
k_p	k_f	k_f	$-k_f + k_b + k_p$	$k_f + k_b$	ω_p	$\omega_p - \omega_0$

Table 4.4

Three kinds of signal waves are observed in the third-order optical process. The phase-conjugated wave $(\omega_s, k_s) = (2\omega_0 - \omega_p, k_f + k_b - k_p)$ is observed when the combination of (l, m, n) is equal to (f, p, b) and to (b, p, f).

$$\hat{G}^R(\omega_s)$$

$$k_s \leftarrow \qquad \leftarrow k_b$$

$$\Gamma_{k_s k_b; k_p k_f}(\omega_s - \omega_p)$$

$$k_f \rightarrow \qquad \rightarrow k_p$$

$$\hat{G}^A(\omega_p)$$
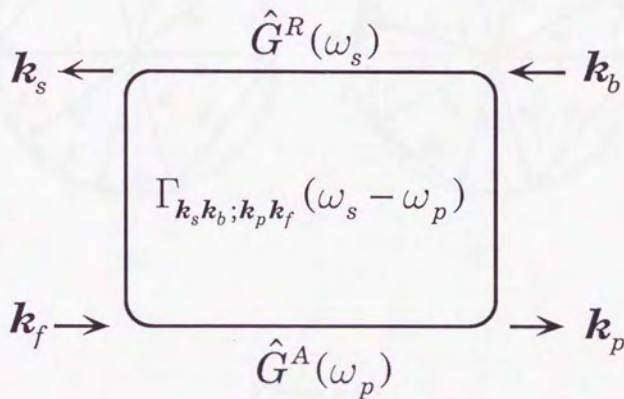
Figure 4.5

The general vertex part working between the retarded and the advanced Green functions. The vertex part depends on the difference of the signal and probe frequency, *i.e.*, $\omega_s - \omega_p$, and on the incident momenta k_f, k_b, and k_p.
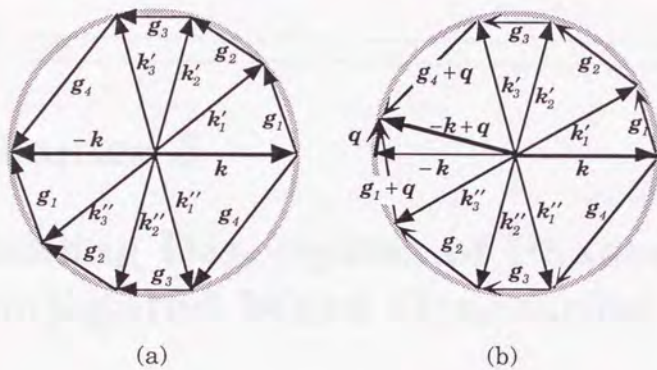
Figure 4.6

Two complementary scattering series producing the enhanced backscattering intensity given by Bergmann [33]. The incident probe wave has the momentum k and the signal wave has the momentum $-k(+q)$. The intermediate states are designated by k_i' and k_i''. The momenta g_i's mean the phase shifts given by the random potential. (a): The two complementary scattering series in the case generating a exactly phase-conjugated wave. The phase shifts given by the random potentials are exactly same between the two scattering series along the upper and lower semicircles. (b): The same scattering processes as given in (a) in the case with a finite momentum deviation q. It is found that the finite momentum deviation reduces the coherence of these complementary scattering processes.

Chapter 5

Scaling Description of Phase-conjugated Wave Generation

5.1 Introduction to Scaling Description

If the disorder in the system increases, the localized-delocalized transition is expected to occur in the three-dimensional system. Such transition point in the frequency domain is called mobility edge ω^*. Since the localization length of the exciton diverges at the exciton mobility edge, the effective transition dipolemoment of an exciton should become very large around the transition point. This gives a very interesting situation, because the nonlinear susceptibility seems to be very sensitive to a spread of the wavefunction, as was seen in Sec. 1.3. In addition, it has been shown in the previous chapter that the phase-conjugated wave generation is playing a special role in the random system. In this chapter, we will investigate the behavior of the nonlinear susceptibility for the phase-conjugated wave generation around the exciton mobility edge. Perturbational treatments such as one presented in the previous chapter breaks down around the exciton mobility edge. For this reason, we will construct the scaling theory [22,23,34,35] of the enhancement factor N_{eff} to examine the behavior of the nonlinear susceptibility around the mobility edge.

Localization effect can be described through the interaction between the two diffusion modes [23,36], and this interaction renormalizes and decreases the diffusion coefficient. General arguments about the renormalization of the diffusion coefficient and the diffusion propagator itself were given in the form of the field theoretical model called (several kinds of) nonlinear sigma models [36–41]. (The treatments of the *original* nonlinear sigma model were mentioned in Refs. [42–44]. Finite size effect in the nonlinear sigma model was given in Refs. [45,46].) In their treatments, the diffusion modes can be formulated as Goldstone modes.

The detailed calculation and renormalization group analysis in the field theoretical model of the Anderson localization will be given in Appendix B.

We begin this chapter with the second lowest order perturbational calculation of the enhancement factor N_{eff} for the phase-conjugated wave generation (Sec. 5.2). This will tell us how the interaction between the two diffusion modes will renormalize the diffusion coefficient and the diffusion propagator. By combining the result by the perturbational calculation and the insight from the field theoretical treatment, we construct the scaling description of N_{eff}. This will enable us to investigate the disorder effect and the finite size effect on the enhancement factor N_{eff} for the phase-conjugated wave generation. In Sec. 5.3 and later, we will systematically evaluate the dependence of the phase-conjugated signal on various physical quantities — randomness, the detuning of the pump- and probe- frequencies from the exciton mobility edge, the misalignment of the two pump beams and the system size (Sec. 5.4). In addition, we will find the spectral singularity in the nonlinear susceptibility around the exciton mobility edge (Sec. 5.5).

5.2 Coherent Volume Function and Renormalized Cooperon

It is straightforward to evaluate the second lowest order contribution for the vertex part $\Gamma(\omega_s - \omega_p)$ [47,48]. This next higher order correction corresponds to the one-loop calculation of the transverse correlation function in the nonlinear sigma model. Here we follow the line of Ref. [47]. The renormalized cooperon channel $\Gamma_c^{(1)}$ can be evaluated by use of the following Dyson equation as

$$\Gamma_c^{(1)}(\delta\omega;\boldsymbol{q}) = \Gamma_c^{(0)}(\delta\omega;\boldsymbol{q}) + \Gamma_c^{(0)}(\delta\omega;\boldsymbol{q})\,\Pi_c^{(1)}(\delta\omega;\boldsymbol{q})\,\Gamma_c^{(1)}(\delta\omega;\boldsymbol{q}). \tag{1}$$

The equation above can be schematically illustrated as shown in Fig. 5.2. We take the leading singular term for $\boldsymbol{q}\approx\boldsymbol{0}$ and $-i\delta\omega+2\gamma\approx 0$. To perform the systematic expansion in W/T or $(4\pi^2 N_0 D_0 \ell^{d-2})^{-1}$, we find that $\Pi_c^{(1)}$ is expressed by the summation of the diagrams as in the Fig. 5.3. Each contribution can be written down explicitly as

$$\Pi_c^{(1)} = \Pi_c^{(1A)} + \Pi_c^{(1B)} + \Pi_c^{(1C)}, \tag{2}$$

where

$$\Pi_c^{(1A)}(\delta\omega;\boldsymbol{q}) = \sum_{\boldsymbol{Q}}\left[\left(\Gamma_d^{(0)}(\delta\omega;\boldsymbol{Q}) - \frac{\gamma'}{\pi N_0}\right)\sum_{\boldsymbol{k}} G_{\boldsymbol{k}+\boldsymbol{q}}^R G_{\boldsymbol{Q}-\boldsymbol{k}}^R G_{\boldsymbol{k}}^A G_{\boldsymbol{Q}-\boldsymbol{k}-\boldsymbol{q}}^A\right], \tag{3a}$$

$$\Pi_c^{(1B)}(\delta\omega;\boldsymbol{q}) = \frac{\gamma'}{\pi N_0}\sum_{\boldsymbol{Q}} \Gamma_d^{(0)}(\delta\omega;\boldsymbol{Q})\left(\sum_{\boldsymbol{k}} G_{\boldsymbol{k}+\boldsymbol{q}}^R G_{\boldsymbol{Q}-\boldsymbol{k}}^R G_{\boldsymbol{k}}^A\right)^2, \tag{3b}$$

$$\Pi_c^{(1C)}(\delta\omega;\boldsymbol{q}) = \frac{\gamma'}{\pi N_0}\sum_{\boldsymbol{Q}} \Gamma_d^{(0)}(\delta\omega;\boldsymbol{Q})\left(\sum_{\boldsymbol{k}} G_{\boldsymbol{k}}^R G_{\boldsymbol{Q}-\boldsymbol{k}}^A G_{\boldsymbol{k}-\boldsymbol{q}}^A\right)^2. \tag{3c}$$

The straightforward evaluation of the integrals leads to

$$\Pi_c^{(1)}(\delta\omega;\boldsymbol{q}) \cong \frac{\pi N_0}{4\gamma'^4} D_0 q^2 \sum_{\boldsymbol{Q}} \Gamma_d^{(0)}(\delta\omega;\boldsymbol{Q}). \tag{4}$$

Thus the renormalized cooperon mode $\Gamma_c^{(1)}(\delta\omega;\boldsymbol{q})$ is expressed by

$$\Gamma_c^{(1)}(\delta\omega;\boldsymbol{q}) = \frac{\gamma'}{\pi N_0}\frac{2\gamma'}{D_0(1-\Delta)q^2 - i\delta\omega + 2\gamma}, \tag{5}$$

$$\Delta = \frac{1}{\pi N_0}\int_{1/L}^{1/\ell} \frac{1}{D_0 Q^2 - i\delta\omega + 2\gamma}\frac{d^d Q}{(2\pi)^d}. \tag{6}$$

The correction Δ is found to be logarithmic in the two-dimensional bulk system as

$$\Delta = \frac{1}{4\pi^2 N_0 D_0}\ln\left[\frac{2\gamma'}{-i\delta\omega + 2\gamma}\right]. \tag{7}$$

This kind of logarithmic correction in the two-dimensional bulk system is characteristic in the localization theory [23,49].

5.3 Scaling Form of the Coherent Volume Function

The form of the renormalized diffusion (cooperon) mode has a more profound meaning than it looks. It shows that all the disorder effect of diffusion modes in the delocalized phase is incorporated through the renormalized diffusion coefficient $D_0(1-\Delta)$. As is shown in framework of the nonlinear sigma model, this nontrivial feature of the Anderson localization theory holds good even if we consider still more higher-order correction, because it is based upon the nonvanishing of the order parameter, *i.e.*, the averaged density of states, at the transition point. The detail will been seen in Appendix B. Since the exciton's average density of states is not expected to vanish at the exciton mobility edge, we rely fairly upon this insight. Hence we take full advantage of this feature. We will apply the length-dependent scaling law of the diffusion coefficient to determine the scaling form of the diffusion (cooperon) mode. This allows us to investigate the disorder effect and the finite size effect on the enhancement factor N_{eff} for phase-conjugated wave generation in terms of the correlation (localization) length ξ.

When the inelastic scattering length $L_\varphi = [N_0(-i\omega_s + i\omega_p + 2\gamma)]^{-1/d}$ is introduced, the enhancement factor N_{eff} and the coherent volume function Ξ_L derived in Eqs. (14) and (15) of Chapter 4 are given by

$$N_{\text{eff}} = \frac{N}{V}\left[1 + \frac{1}{d}\frac{\partial}{\partial \ln L_\varphi}\right]\Xi_L, \tag{8}$$

$$\Xi_L = \frac{1}{N_0 D_L(q^2 + L^{-2}) + L_\varphi^{-d}}. \tag{9}$$

Here we omit the numerical factor $2/\pi$ as we are discussing only the order of magnitude. In Eq. (9), we carefully replaced q^2 by $q^2 + L^{-2}$ in the denominator,

because all the momenta are discretized and cut off by the order of $1/L$ in the sample with finite volume $V = L^d$. The renormalized diffusion coefficient D_L depends upon L, q and L_φ, as will be discussed in the following. The length-dependent scaling theory [22] allows us to estimate the renormalized diffusion coefficient in terms of the dimensionless conductance $g_L = L^{d-2}N_0 D_L$. The dimensionless conductance g_L is determined by the following relation in the weakly localized regime:

$$L\frac{d\ln g_L}{dL} = \beta(g_L) = (d-2) - \frac{1}{g_L} + \cdots \tag{10}$$

On the right hand side of the equation above, we have made use of the result obtained by the expansion in $\epsilon = d - 2$. Thus we obtain

$$N_0 D_L = g_{L'}(L')^{2-d} = g^*\left[(L')^{2-d} + (\xi)^{2-d}\right] \tag{11}$$

on the delocalized side of the exciton mobility edge, where g^* is given by $1/(d-2)$. The length ξ is the correlation (localization) length determined only by the elastic scattering. The length L' is the effective linear size of the system that $N_0 D_L$ is scaled up to. The length L' can be evaluated to be equal to $\min[L, q^{-1}, \tilde{L}_\varphi]$, where $\tilde{L}_\varphi$ is a length defined by $\tilde{L}_\varphi \equiv \sqrt{D/(-i\omega_s + i\omega_p + 2\gamma)}$. (D is a renormalized diffusion coefficient.) The relation among $\tilde{L}_\varphi$, L_φ and ξ will be given in Appendix B. It will be shown that $\tilde{L}_\varphi$ and L_φ will be shown to be related by $\tilde{L}_\varphi \approx (g^*)^{1/d} L_\varphi$ around the mobility edge (*i.e.*, $L_\varphi \ll \xi$).* The correlation (localization) length ξ diverges at the mobility edge like $|\omega - \omega^*|^{-\nu}$ [23,50,51]. The critical exponent ν must be larger than $2/d = 0.666\cdots$ by the Chayes and

---

* By contrast, $\tilde{L}_\varphi$ is given by $(g^*)^{1/2} L_\varphi \sqrt{L_\varphi/\xi}$ in the delocalized limit, *i.e.*, $\xi \ll L_\varphi$. See Appendix B for the detail.

Chayes theorem [52]. The realistic value of the critical exponent ν is between 0.73 (by ϵ-expansion with Borél-Padé analysis [53]) and ~ 1.5 (by numerical analysis [54]).

In the following, we shall consider only the three-dimensional case where the localized-delocalized transition is believed to occur. As a result, we obtain the expression for Ξ_L on the delocalized side of the transition from Eqs. (9) and (11) as

$$\Xi_L = \left[\left(\frac{1}{\min[L, \tilde{L}_\varphi, q^{-1}]} + \frac{1}{\xi} \right) (q^2 + L^{-2}) + L_\varphi^{-3} \right]^{-1}. \tag{12}$$

We discuss all the effects due to disorder, misalignment, and finiteness of the sample size, based upon Eq. (12). In the large volume limit, the behavior of N_{eff} for the phase-conjugated signal obtained from Eq. (12) is identical to that obtained in Ref. [12]. We are mainly concerned with the behavior of the enhancement factor around the mobility edge, where $\tilde{L}_\varphi$ becomes of a comparable order of L_φ.

5.4 Sample Size Dependence

In this section, we investigate the sample size dependence of the coherent volume function Ξ_L in the case $\boldsymbol{q} = \boldsymbol{k}_f + \boldsymbol{k}_b = \boldsymbol{0}$ on both sides of the exciton mobility edge. First we examine the behavior of Ξ_L on the delocalized side. As is easily confirmed from Eq. (12), the coherent volume function Ξ_L is proportional to L^3 in small linear size. The larger the linear size becomes, the more deviates the coherent volume function from the cubic power law and at last it is saturated to the constant value L_φ^3 as shown in Figs. 5.4 and 5.5. This crossover occurs at $L \sim \tilde{L}_\varphi$ and the behavior in the intermediate (mesoscopic) region is also highly

dependent on the size of the correlation length ξ, as the solid lines in Fig. 5.4 show. Figure 5.5 is a logarithmic pot of Fig. 5.4. Because of the saturation of the large volume limit, the behavior of the coherent volume function Ξ_L is deviated from the cubic power dependence of L. In the figure, we also plot $L^{2.6}$ function, which was observed by the experiment in Ref. [55]. The result obtained by the scaling theory is likely to fit so well.

We now go on to the behavior on the localized side of the transition. When the localization length ξ is larger than the effective linear size $L' = \min[L, q^{-1}, \bar{L}_\varphi]$, we cannot distinguish between the localized state and the delocalized state, so that we expect that the behavior on the localized side is similar to that on the delocalized side. However, when the localization length is smaller than $L' = \min[L, q^{-1}, \bar{L}_\varphi]$, the difference between the localized and delocalized sides emerges. We can estimate Ξ_L on the localized side by following the scaling law away from initial point near the fixed point up to a length scale $L = \xi$ [56]. As a result, we expect that the coherent volume function Ξ_L on the localization sides proportional to L^3 in the small volume limit and saturated to ξ^3, not to L_φ^3, as Fig. 5.3 shows.

5.5 Spectral Anomaly and Misalignment Dependence around Exciton Mobility Edge

Next we illustrate the expected behavior of N_{eff} in the unit of N/V as a function of ξ^{-1} and q in Figs. 5.6 and 5.7. Since the correlation (localization) length ξ is proportional to $|\omega - \omega^*|^{-\nu}$, Fig. 5.6 shows the anomalous ω-dependence

of the enhancement factor N_{eff} around the exciton mobility edge ω^* with the fixed misalignment q. Just near the transition point, the singularity is cut off by $\sim 2L_\varphi^3$ both on the sides. Away from the transition point, N_{eff} decreases as $\xi^3 \propto |\omega - \omega^*|^{-3\nu}$ on the localized side, and as $\xi/q^2 \propto |\omega - \omega^*|^{-\nu}$ on the delocalized side, which makes the spectrum non-symmetric on the tails. As shown by Fig. 5.4, it should be noted that when the misalignment q approaches zero, the region where N_{eff} is dominated by the length scale L_φ is much larger on the delocalized side. The background intensity comes from the terms neglected in our treatment. The relative value of the peak to the background is of the order of $(L_\varphi / \xi_{\text{coh}})^3 \sim \gamma'/\gamma \, (\gg 1)$ at the mobility edge.

In Fig. 5.7, the enhancement factor N_{eff} is drawn as a function of the misalignment of the pump beams q. In the region so closed to the exciton mobility edge that the correlation (localization) length ξ becomes larger than the characteristic wavelength q^{-1} and the inelastic scattering length $\tilde{L}_\varphi$, the localized and delocalized states cannot be distinguished as shown by the solid line in Fig. 5.7. Away from the exciton mobility edge, where $\xi \leq q^{-1}$, there will emerge the difference in the q-dependence of the enhancement factor N_{eff} on the delocalized side (the dash line) and on the localized side (the dotted dash line) in the region of $q \leq \tilde{L}_\varphi^{-1}$, as is shown in Fig. 5.7. The width of the peak in Fig. 5.7 in the delocalized phase is characterized by $\tilde{L}_\varphi^{-1}$, which is almost equal to $\sqrt{\xi/(L_\varphi)^3}$ in the delocalized limit, and to $(L_\varphi)^{-1}$ around the mobility edge ω^*.

5.6 Summary of the Scaling Description of PCW Generation

In this chapter, we have constructed the scaling description of the

enhancement factor N_{eff} for the phase-conjugated wave generation. To evaluate the renormalized cooperon mode, we have applied the length-dependence scaling theory of the diffusion coefficient into the diffusion propagator. The validity of this application is justified by the next lowest-order calculation of the cooperon mode and the field theoretical treatment of the Anderson localization. The scaling description have enabled us to investigate systematically how the enhancement factor for the phase-conjugated wave generation depends upon randomness, the misalignment of the two pump beams, the detuning of the probe- and pump- frequencies from ω^*, and the system size. Our scaling theory have reproduced the confinement effect of the exciton in the small volume region and also shown the breakdown of it, as in Fig. 5.4 and 5.5. We have also found the spectral anomaly and enhancement of the nonlinear susceptibility around the exciton mobility edge, as in Fig. 5.6. In addition, we have investigated the misalignment dependence of the enhancement factor for the phase-conjugated wave generation as in Fig. 5.7.
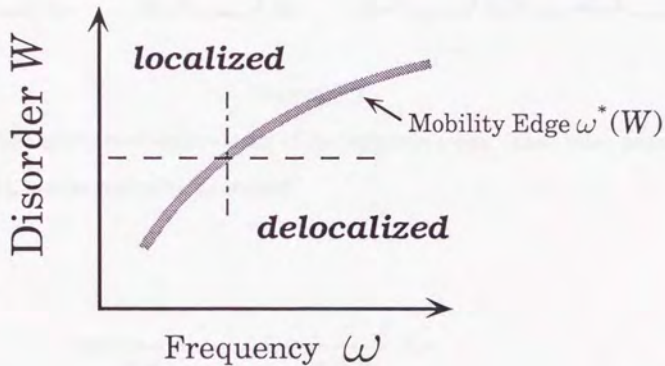
Figure 5.1

Schematic view of the localized and delocalized phases as a function of disorder and the frequency. The grey thick line is the boundary between the localized phase and the delocalized phase. If the disorder increases with a fixed frequency (the dotted dash line), there is a phase transition between the delocalized phase and the localized phase. Similarly, if the frequency is varied with a fixed disorder (the dash line), there is a phase transition between the two phases in frequency domain.
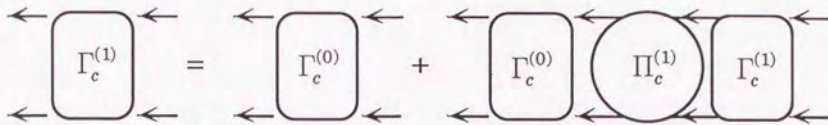
Figure 5.2

Construction of the next higher order of the cooperon mode. The Dyson equation
i.e., Eq. (1), is schematically illustrated.
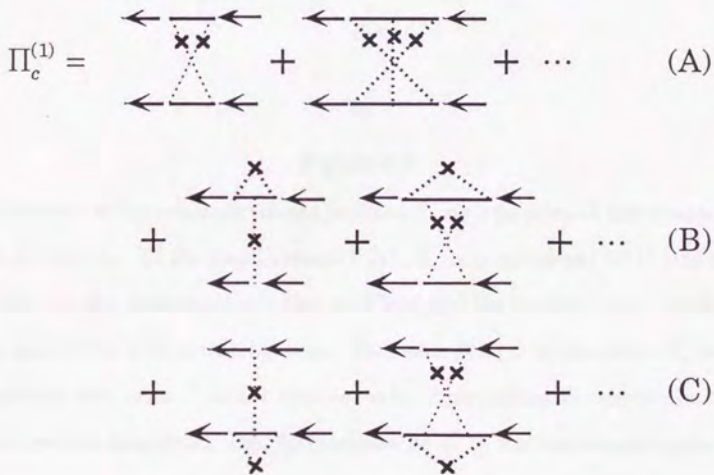
Figure 5.3

Diagrammatic representation of $\Pi_c^{(1)}$ in Figure 5.2 and in Eqs. (2) and (3). The
contributions from the series of diagrams (A), (B), and (C) are written, respectively,
by $\Pi_c^{(1A)}$, $\Pi_c^{(1B)}$, and $\Pi_c^{(1C)}$.
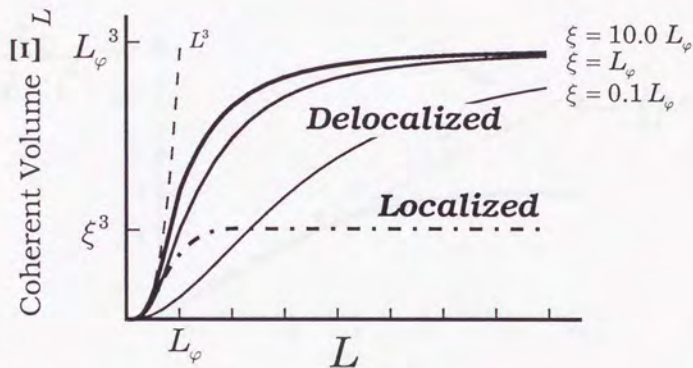
Figure 5.4

The behavior of the coherent volume function Ξ_L as a function of the sample size L at $\boldsymbol{q} = \boldsymbol{k}_f + \boldsymbol{k}_b$. In the small volume limit, Ξ_L is proportional to L^3 (the dash line) both in the delocalized side (the solid line) and the localized side (the dotted dash line) of the exciton mobility edge. The value of Ξ_L is saturated to L_φ^3 on the delocalized side, or to ξ^3 on the localized side. Approaching the exciton mobility edge from the delocalized side, Ξ_L increases as L^3 in the mesoscopic region but always saturated to L_φ^3 in the large volume limit both on the localized and delocalized sides.
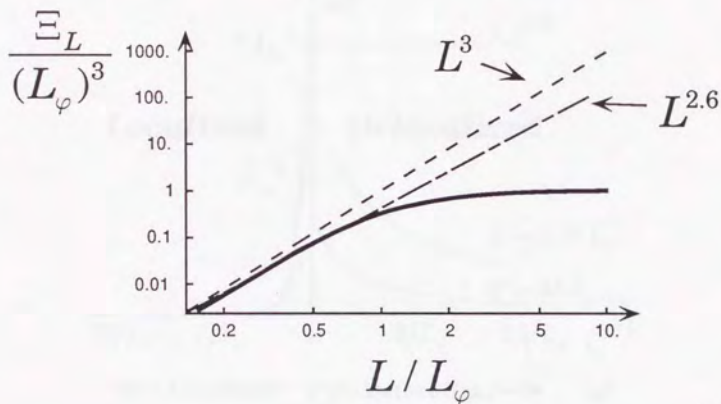
Figure 5.5

Logarithmic plot of the coherent volume function Ξ_L as a function of the logarithm of L/L_φ. Though Ξ_L is proportional to L^3 in the small volume region, the exponent of Ξ_L seems to be slightly deviated from 3 because of saturation in the large volume region. In the figure, the experimental value of the exponent 2.6 by Masumoto, Yamazaki, and Sugawara (1988) [55] is also drawn for the sake of reference.

$$N_{\text{eff}}$$

$$q' \equiv \sqrt{q^2 + L^{-2}}$$

$$q' = 0$$

$$2L_\varphi{}^3$$

Localized   **Delocalized**

$$L_\varphi{}^3$$

$$q' = 0.5/L_\varphi$$

$$q' = 1/L_\varphi$$

$$10/L_\varphi \quad 5/L_\varphi \quad 0 \quad 5/L_\varphi \quad 10/L_\varphi \quad \xi^{-1}$$

$$\longleftarrow \text{Localized} \longrightarrow \hspace{-0.2em} \longleftarrow \text{Delocalized} \longrightarrow \quad \omega$$

$$\omega^*$$
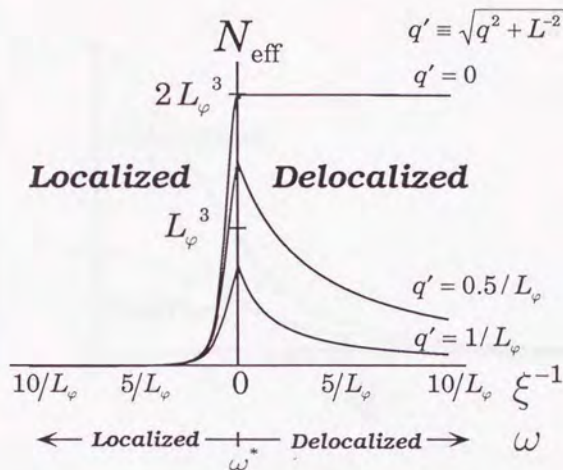
Figure 5.6

The schematic behavior of the enhancement factor N_{eff} for the phase-conjugated wave generation as a function of the inverse of the correlation (localization) length $\xi^{-1} \propto |\omega - \omega^*|^\nu$. The enhancement factor N_{eff} is measured in the unit of N/V with several fixed values of the misalignment of the forward and backward pump beams $\boldsymbol{q} = \boldsymbol{k}_f + \boldsymbol{k}_b$. The system size is assumed to be so large as $L \gg q^{-1}, L_\varphi$ in the figure. Since ξ is given by $\ell |(\omega - \omega^*)/\omega^*|^{-\nu}$, the figure corresponds to the spectrum anomaly around the mobility edge ω^*. On the localized side, N_{eff} decreases by $N_{\text{eff}} \sim \xi^3$, whereas N_{eff} does by $N_{\text{eff}} \sim \xi/q^2$ on the delocalized side, when the pumping frequency is far away from ω^*.
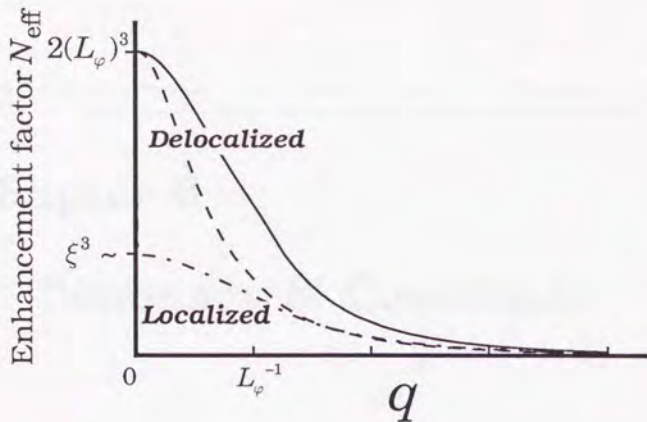
Figure 5.7

The schematic behavior of the enhancement factor N_{eff} for the phase-conjugated wave generation as a function of the misalignment of the forward and backward pump beams $\boldsymbol{q} = \boldsymbol{k}_f + \boldsymbol{k}_b$. The enhancement factor N_{eff} is measured in the unit of N/V with several fixed values of the correlation (localization) length ξ, and the system size is assumed to be so large as $L \gg q^{-1}, L_\varphi$ in the figure. Just near the exciton mobility edge (the solid line), the delocalized and the localized states cannot be distinguished. Away from the exciton mobility edge, the discrimination emerges between the delocalized side (the dash line) and the localized side (the dotted dash line) for $q \le L_\varphi^{-1}$. The width of the peak in the delocalized phase is characterized by $(\tilde{L}_\varphi)^{-1}$, which is almost equal to $\sqrt{\xi/(L_\varphi)^3}$ in the delocalized limit, and to $(L_\varphi)^{-1}$ around the mobility edge. (See also Appendix B.)

Chapter 6

Summary & Conclusion

In this thesis, we have investigated linear and nonlinear susceptibilities under nearly resonant pumping of the Frenkel excitons in disordered system. We have introduced the model in which we can take full account of the dephasing process correctly from the microscopic point of view. Particular attention have been paid to the nonlinear susceptibility generating the phase-conjugated wave in the random system. We have evaluated the linear and nonlinear susceptibilities by the perturbational calculation as to the electron-radiation interaction. As a result, we have clarified that the phase-conjugation plays a special role in the random system, and that it is closely related to the exciton's diffusive motion.

In this paper, we have constructed the scale description of the phase-conjugated wave generation and investigated the behavior of the enhancement factor N_{eff} for phase-conjugated wave generation on both sides of the exciton mobility edge. In small volume region, our theory reproduces the result of the confinement effect. For the larger volume crystal, the qualitative difference between the delocalized state and the localized state has been manifested. The expected singular behavior of the spectrum around the exciton mobility edge has also been demonstrated as a function of pumping frequency and the misalignment of the two pump beams.

Based upon the obtained results in the paper, we can propose two kinds of experiments to observe the singular behavior of $\chi^{(3)}$ near the exciton mobility edge ω^*. Here we confine ourselves to the case of exactly degenerate four-wave mixing in a large crystal, *i.e.*, $\omega_0 = \omega_p \equiv \omega$ in the system with $L \gg L_\varsigma, q^{-1}$. First when we have the finite misalignment $\boldsymbol{q} = \boldsymbol{k}_f + \boldsymbol{k}_b$ fixed, the singular behavior of the generation of phase-conjugated wave like $N_{\text{eff}} = (N/V)\xi q^{-2} \propto |\,\omega - \omega^*\,|^{-\nu}$ can be

observed as a function of pump frequency ω on the delocalized side for $\xi \lesssim q^{-1} \lesssim \tilde{L}_\varphi$. When the pump frequency ω_0 is detuned from the exciton mobility edge ω^* on the localized side, the signal will decay more rapidly as $N_{\text{eff}} = (N/V)\xi^3 \propto |\omega - \omega^*|^{-3\nu}$. This dependence of the signal on the pump frequency is saturated in so close pumping region as $\tilde{L}_\varphi^{-1} \gtrsim q$ on the delocalized side, or as $\xi \gtrsim L_\varphi$ on the localized side. This crossover will be able to determine the absolute value of the correlation and localization length $\xi = \xi_0 |(\omega - \omega^*)/\omega^*|^{-\nu}$.

Second when the detuning $|\omega - \omega^*|$ is fixed on the delocalized or localized sides, the correlation or localization length ξ will be determined by changing the misalignment q. In pumping localized excitons, the enhancement factor N_{eff} is saturated to the value $(N/V)\xi^3 \propto |\omega - \omega^*|^{-3\nu}$ for the smaller misalignment $q \lesssim \xi^{-1}$, whereas it decreases as q^{-3} for the larger misalignment $q \gtrsim \xi^{-1} \gtrsim L_\varphi^{-1}$. By observing this crossover, we will be able to determine the localization length ξ as a function of ω. On the other hand, when the misalignment q decreases on the delocalized side, the enhancement factor N_{eff} for the phase-conjugated signal increases as q^{-3} for $q \gtrsim \xi^{-1} \gtrsim L_\varphi^{-1}$ or as q^{-2} for $\xi^{-1} \gtrsim q \gtrsim \tilde{L}_\varphi^{-1}$ and saturated to the value $N_{\text{eff}} = (N/V)L_\varphi^3$ for the smaller misalignment $q \lesssim \tilde{L}_\varphi^{-1}$. The crossover at $q \sim \tilde{L}_\varphi^{-1}$ depends on the detuning $|\omega - \omega^*|$. Hence we expect the singular enhancement of the third-order optical processes, *i.e.*, the generation of phase-conjugated wave near the exciton mobility edge. In the reverse way of thinking, we will be able to study the localized-delocalized transition of an exciton by observing the singular spectrum of phase-conjugated wave generation as a function of pump- and probe-frequency around the exciton mobility edge ω^* and the misalignment of the forward and backward beams.

We will mention miscellaneous effects which we have neglected so far. First is about the renormalization of the inelastic relaxation rate near the transition point. As inelastic processes, we take relaxation by phonons. There was no renormalization of the relaxation rate of the exciton's energy γ, as was shown in Chapter 5. If the radiative relaxation is a dominant channel of the energy relaxation, this assumption is not valid, so we have taken the situation where the energy relaxation processes through phonons give a dominant contribution to the inelastic relaxation rate. Since the relaxation rate due to phonons are determined approximately by a spread of the wavefunction, inelastic relaxation rate seems to be a slow varying function of the disorder around the localized-delocalized transition. As we have mentioned in Sec. 5.3 and Appendix B, another renormalization constant Z would be needed within the framework of the nonlinear sigma model, if there were any renormalization of the inelastic relaxation rate, and it would lead to the vanishing of the exciton's density of the states at the transition point. Though the incorporation of such effect may be possible, as in the renormalization group theory in the disordered interacting system [63–66], we think the vanishing of the density states in the exciton system is rather strange.

Another problem is about the validity of the one-parameter scaling theory of the Anderson transition itself, which our present treatment heavily relies upon. Extensive numerical studies of the Anderson localization to confirm the one-parameter scaling theory have been performed in the center of the band. However, the critical behavior near the band edge is complicated and still have some ambiguity. Many authors have obtained the mobility edge trajectory as a

function of the disorder and the energy by numerical methods [54,67–69] and by analytical methods[*] [70–73]. In Fig. 6.1, the mobility edge trajectory calculated numerically by Bulka *et. al.* [69] is shown. (The symbol V is the transfer between the nearest-neighbor sites, which we designate by T so far). From Fig. 6.1 and data obtained by other authors, it appears that one-parameter scaling theory of the Anderson transition can be applied within the energy region which corresponds to the band of the undisordered system, *i.e.*, $|E| \leq 6V$ in Fig. 6.1. However, in the energy region outside the band of the undisordered system, *i.e.*, $|E| \gtrsim 6V$ in Fig. 6.1, the effect of the potential localization is as important as the quantum interference effect. There is some region slightly outside the undisordered band where the localized-delocalized-localized transition will occur with a fixed energy and increasing the disorder. In this situation, our scaling theory is relevant to the second transition (from delocalization to localization with a fixed energy and increasing disorder), because this transition seems to be caused by the quantum interference effect. Though the whole behavior of the mobility edge trajectory may be explained by the quantum interference effect with the effect of the disorder-induced band shift, the critical behavior at the transition from the localized state to the delocalized state with *increasing* disorder is not clarified so far.

Finally we will check the experimental data to confirm the possibility of the localized-delocalized transition of the exciton. Bearing Z_3 excitons of CuCl

---

[*] Licciardello and Economou [70] used the localization-function method to determine the mobility edge. Economou and Soukoulis [71–72] expoited what is called the potential-well analog with the aid of the coherent potential approximation. Kotov and Sadovskii [73] extended the self-consistent theory introduced by Vollhardt and Wölfle [50].

crystals in mind[*], we use the lattice constant $a = 0.54$ [nm], the resonant wave number $k_0 \cong 4.5 \times 10^5$ [cm^{-1}], and the exciton's effective mass $m = 3.14\, m_0$. The exciton Bohr radius of Z_3 excitons is $a_B = 0.70$ [nm], so it doesn't so bad to treat them as Frenkel excitons. To justify our theoretical treatment, the value of the dephasing rate γ_c' at the exciton mobility edge should be larger than the inelastic relaxation rate γ. To estimate the order of γ_c', the Ioffe-Regel condition[†] is useful. This condition gives $\gamma_c' \sim 1$ [meV], which justifies our basic assumption $\gamma_c' \gg \gamma$. In addition, this order of the dephasing rate is experimentally attainable. If we use the numerical results of the mobility edge by Ref. [54,69], we can get more information upon the dependence on the kind of the energy distribution (Gaussian, box, and Lorentzian). Using Eq. (5) in Chapter 4 and taking $N_0 \approx 10^{20}$ [cm^{-3} eV^{-1}], γ_c' can be estimated to be $3 \sim 6$ [meV] (Gaussian), $12 \sim 25$ [meV] (box), and $0.005 \sim 0.01$ [meV] (Lorentzian) at the band edge of the system without disorder. Thus the Gaussian and box distribution models can be valid, but the Lorentzian distribution model cannot be allowed to use the scaling theory of the Anderson transition. The inelastic scattering length is given $L_\varphi \approx 6.3 \times 10^{-6}$ [cm], so by adjusting the impurity concentration, or the pump frequency, the phase-conjugated wave generation may be enhanced by the factor $(L_\varphi / \xi_{coh})^3 \sim 10^2$, compared with the third-order susceptibility for the other processes.

---

[*] The localized-delocalized transition of the $(CuCl)_{1-x}(CuBr)_x$ solution is a suggested example to apply our scaling theory.

[†] The localized-delocalized transtion will happen when the mean free path ℓ is nearly equal to the lattice constant a.
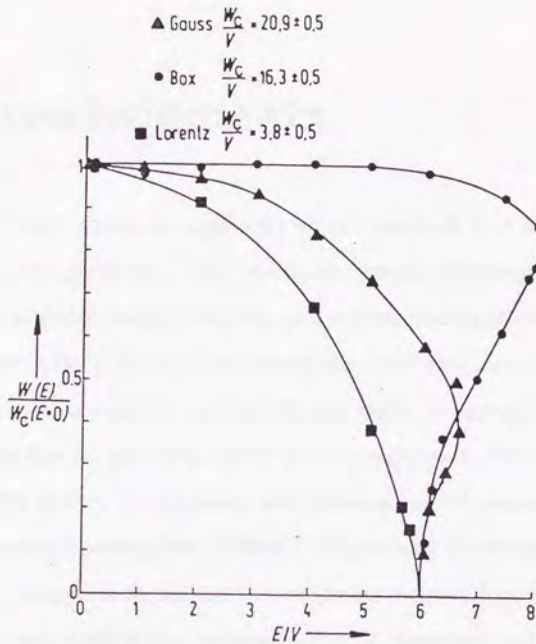
Figure 6.1

Mobility edge trajectories $W_c(E)$ as a function of the disorder and the energy for the box ($\bullet$), Gaussian ($\blacktriangle$), and Lorentzian ($\blacksquare$) distribution of onsite energies. The result was obtained numerically by B. Bulka, *et. al.* (1987) (Ref. [69]). The symbol V is the dipolar interaction between the nearest-neighboring sites, which we have designated by T throughout the thesis. The energy $E = 6V$ equals to the band edge of the system without disorder. The critical disorder for each distribution at the center of the band is $W_c(0)/V = 16.3 \pm 0.5$ (box $- \bullet$), $W_c(0)/V = 20.9 \pm 0.5$ (Gaussian $- \blacktriangle$), and $W_c(0)/V = 3.8 \pm 0.5$ (Lorentzian $- \blacksquare$).

Acknowledgments

The author wishes to express his sincere thanks to Prof. E. Hanamura for suggesting the problems of the nonlinear optical phenomena, stimulating discussions at every stage of the work, and critical reading of a manuscript. He wishes to thank Dr. T. Tokihiro for encouraging and fruitful discussion particularly about the theory of nonlinear optics. He also wishes to express his gratitude to Prof. N. Nagaosa for providing many valuable discussion. The author's special thanks is due to Prof. M. Gonokami for providing helpful comments and advice from experimental point of view, to Prof. T. Fujiwara for their valuable comments, to Prof. H. Fukuyama for critical comments and helpful discussions about the localization theory. He is also indebted to Prof. A. Kawabata and Prof. S. Hikami for providing their casual comments and explanation about the theory of the Anderson localization. Finally thanks are due to all the members belonging to Rikigaku Kyoshitsu for their hospitality given to him.

References

[1] M. Ueta, H. Kanzaki, K. Kobayashi, Y. Toyozawa, and E. Hanamura, *"Excitonic Processes in Solids"*, Springer-Verlag (1986).

[2] E. Hanamura, "Very large optical nonlinearity of semiconductor microcrystallites" Phys. Rev. B **37**(3), 1273–1279 (1988).

[3] E. Hanamura, "Rapid radiative decay and enhanced optical nonlinearity of excitons in a quantum well" Phys. Rev. B **38**(2), 1228–1234 (1988).

[4] F.C. Spano and S. Mukamel, "Nonlinear susceptibilities of molecular aggregates: Enhancement of $\chi^{(3)}$ by size" Phys. Rev. A **40**(15), 5783–5801 (1989).

[5] F.C. Spano and S. Mukamel, "Cooperative Nonlinear Optical Response of Molecular Aggregates: Crossover to Bulk Behavior" Phys. Rev. Lett. **66**(9), 1197–1201 (1991).

[6] J. Knoester and S. Mukamel, "Transient gratings, four-wave mixing and polariton effects in nonlinear optics" Phys. Rep. **205**(1), 1–58 (1991).

[7] J. Feldmann, G. Peter, E.O. Göbel, P. Dawson, K. Moore, and C. Foxon, "Linewidth Dependence of Radiative Exciton Lifetimes in Quantum Wells" Phys. Rev. Lett **59**(20), 2337–2340 (1987).

[8] E. Hanamura "Superradiative decay and enhanced optical nonlinearity of low-dimensional excitons". In *SPIE: Applications of Ultrashort Laser Pulses in Science and Technology,* Society of Photo Optical Instrumentation Engineers, 1990, pp. 96–105.

[9] E. Hanamura, "Weak localization of polaritons and the generation of phase-conjugated light waves" Phys. Rev. B **39**(2), 1152–1163 (1989).

[10] V.E. Kravtsov, V.I. Yudson, and V.M. Agranovich, "Theory of phase conjugation of light in disordered nonlinear media" Phys. Rev. B **41**(5), 2794–2799 (1990).

[11] V.I. Yudson and P. Reineker, "Theory of optical phase conjugation in

disordered media: Coherent properties of the backscattered field" Phys. Rev. B **45**(5), 2073–2078 (1992).

[12] N. Taniguchi and E. Hanamura, "Singular enhancement of phase-conjugated wave generation near the mobility edge of exciton" Phys. Lett. A (to be published)

[13] N. Taniguchi and E. Hanamura, "Localized-Delocalized Transition of Exciton Studied by Generation of Phase-Conjugated Waves" Solid State Commun. **85**(10), 843–848 (1993).

[14] N. Taniguchi and E. Hanamura, "Localized-delocalized transition of the exciton and scaling description of phase-conjugated wave generation" Phys. Rev. B **47** (May 15, 1993).

[15] V.E. Kravtsov, V.M. Agranovich, and K.I. Grigorishin, "Theory of second-harmonic generation in strongly scattering media" Phys. Rev. B **44**(10), 4931–4942 (1991).

[16] D. Bennhardt, P. Thomas, A. Weller, M. Lindberg, and S.W. Koch, "Influence of Coulomb interaction on the photon echo in disordered semiconductors" Phys. Rev. B **43**(11), 8934–8945 (1991).

[17] Y. Tokura, T. Koda, and I. Nakada, "Exciton Dynamics in Isotopically Mixed Crystals of Anthracene" J. Phys. Soc. Jpn. **47**(6), 1936–1947 (1979).

[18] S. Chu, H.M. Gibbs, S.L. McCall, and A. Passner, "Energy Transfer and Anderson Localization in Ruby" Phys. Rev. Lett. **45**(21), 1715–1718 (1980).

[19] J. Hegarty, L. Goldner, and M.D. Sturge, "Localized and delocalized two-dimensional excitons in GaAs-AlGaAs multiple-quantum-well structures" Phys. Rev. B **30**(12), 7346–7348 (1984).

[20] V.M. Agranovich, V.E. Kravtsov, and I.V. Lerner, "On the possibility of photon localization in doped semiconductors near excitonic resonances" Phys. Lett. **A125**(8), 435–440 (1987).

[21] S.T. Cundiff, H. Wang, and D.G. Steel "Polarization dependent Coherent Nonlinear Spectroscopy: A Probe of Exciton Localization in Quantum Wells". In *International Conference on Quantum Electronics Technical Digest Series 1992, Vol. 9,* Vienna, 1992.

[22] E. Abrahams, P.W. Anderson, D.C. Licciardello, and T.V. Ramakrishnan, "Scaling Theory of Localization: Absence of Quantum diffusion in Two Dimensions" Phys. Rev. Lett. **42**(10), 673–676 (1979).

[23] P.A. Lee and T.V. Ramakrishnan, "Disordered electronic systems" Rev. Mod. Phys. **57**(2), 287–337 (1985).

[24] R.F. Loring and S. Mukamel, "Extra resonances in four-wave mixing as a probe of exciton dynamics: the steady-state analog of the transient grating" J. Chem. Phys. **84**(3), 1228–1242 (1986).

[25] Y.R. Shen, *"the Principles of Nonlinear Optics"*, Wiley-Interscience, New York (1984).

[26] M. Schreiber and Y. Toyozawa, "Numerical Experiments on the Absorption Lineshape of the Exciton under Lattice Vibrations. I. The Overall Lineshape." J. Phys. Soc. Jpn. **51**(5), 1528–1536 (1982).

[27] H. Fidder and D.A. Wiersma, "Resonance-Light-Scattering Study and Line-Shape Simulation of the J Band" Phys. Rev. Lett. **66**(11), 1501–1504 (1991).

[28] E. Hanamura, "Effects of trapped states on spectra of four-wave mixing and differential transmission" Phys. Rev. B **46**(8), 4718–4713 (1992).

[29] F.C. Spano, "Fermion Excited States in One-Dimensional Molecular Aggregates with Site Disorder: Nonlinear Optical Response" Phys. Rev. Lett. **67**(24), 3424–3427 (1991).

[30] F.C. Spano, "Fermion Excited States in One-Dimensional Molecular Aggregates with Site Disorder: Nonlinear Optical Response" Phys. Rev. Lett. **68**(19), 2976(E) (1992).

[31] J. Knoester, "Nonlinear Optical Susceptibilities of Disordered Aggregates: A Comparison of Schemes to Account for Intermolecular Interactions" Phys. Rev. A, (to be published) (1993).

[32] E. Lieb, T. Schultz, and D. Mattis, "Two Soluble Models of an Antiferromagnetic Chain" Ann. Phys. **16**, 407–466 (1961).

[33] G. Bergmann, "Weak localization in thin films — a time-of-flight experiment with conduction electrons" Phys. Rep. **107**(1), 1–58 (1984).

[34] A. Kawabata, "Scaling Theory of Anderson Localization" Prog. Theor. Phys.

Suppl. **84**, 16–46 (1985).

[35] S. Hikami, "Anderson Localization and Nonlinear σ Model" Prog. Theo. Phys. Suppl. **84**, 120–137 (1985).

[36] K.B. Efetov, A.I. Larkin, and D.E. Khmel'nitskii, "Interaction of diffusion modes in the theory of localization" Sov. Phys. JETP **52**(3), 568–574 (1980).

[37] F. Wegner, "The mobility edge problem: Continuous symmetry and a conjecture" Z. Phys. **B35**, 207–210 (1979).

[38] L. Schäfer and F. Wegner, "Disordered System with n Orbitals per Site: Lagrange Formulation, Hyperbolic Symmetry, and Goldstone Modes" Z. Phys. **B38**, 113–126 (1980).

[39] S. Hikami, "Anderson localization in a nonlinear-σ-model representation Phys. Rev. B **24**(5), 2671–2679 (1981).

[40] A.J. McKane and M. Stone, "Localization as an Alternative to Goldstone's Theorem" Ann. Phys. **131**, 36–55 (1981).

[41] K.B. Efetov, "Supersymmetry and theory of disordered metals" Adv. Phys. **32**(1), 53–127 (1983).

[42] E. Brézin and J. Zinn-Justin, "Spontaneous breakdown of continuous symmetries near two dimensions" Phys. Rev. B **14**, 3110–3120 (1976).

[43] D.R. Nelson and R.A. Pelcovits, "Momentum-shell recursion relations, anisotropic spins, and liquid crystals in $2+\epsilon$ dimensions" Phys. Rev. B **16**(5), 2191–2199 (1977).

[44] J. Zinn-Justin, *"Quantum Field Theory and Critical Phenomena"*, Oxford (1989).

[45] E. Brézin, "An investigation of finite size scaling" J. Physique **43**, 15–22 (1982).

[46] E. Brézin and J. Zinn-Justin, "Finite Size Effects in Phase Transitions" Nucl. Phys. **B257[FS14]**, 867–893 (1985).

[47] E. Abrahams and P.A. Lee, "Scaling Description of the Dielectric Function near the Mobility Edge" Phys. Rev. B **33**, 683–689 (1986).

[48] A. Kawabata, "A self-consistent treatment of Anderson localization" Solid State Commun. **38**, 823–825 (1981).

[49] L.P. Gor'kov, A.I. Larkin, and D.E. Khmel'nitskii, "Particle conductivity in a two-dimensional random potential" JETP Lett. **30**(4), 228–232 (1979).

[50] D. Vollhardt and P. Wölfle, "Diagrammatic, self-consistent treatment of the Anderson localization problem in $d \geq 2$" Phys. Rev. B **22**(10), 4666–4679 (1980).

[51] D. Vollhardt and P. Wölfle, "Scaling Equations from a Self-consistent Theory of Anderson Localization" Phys. Rev. Lett. **48**(10), 699–702 (1982).

[52] J.T. Chayes, L. Chayes, D.S. Fisher, and T. Spencer, "Finite-Size Scaling and Correlation Lengths for Disordered Systems" Phys. Rev. Lett. **57**(24), 2999–3002 (1986).

[53] S. Hikami, "Localization, Nonlinear σ Model and String Theory" Prog. Theo. Phys. Suppl. **107**, 213–227 (1992).

[54] B. Kramer, K. Broderix, A. MacKinnon, and M. Schreiber, "The Anderson Transition: New Numerical Results for the Critical Exponents" Physica **A167**, 163–174 (1990).

[55] Y. Masumoto, M. Yamazaki, and H. Sugawara, "Optical nonlinearities of excitons in CuCl microcrystals" Appl. Phys. Lett. **53**(16), 1527–1529 (1988).

[56] Y. Imry, Y. Gefen, and D.J. Bergman, "Dielectric anomalies near the Anderson metal-insulator transition" Phys. Rev. B **26**(6), 3436–3439 (1982).

[57] N.D. Mermin and H. Wagner, "Absence of ferromagnetism or antiferromagnetism in one- or two-dimensional isotropic Heisenberg models" Phys. Rev. Lett. **17**(22), 1133–1136 (1966).

[58] S. Coleman, "There are no Goldstone Bosons in Two Dimensions" Commun. Math. Phys. **31**, 259–264 (1973).

[59] D.J. Amit, *"Field Theory, the Renormalization Group and Critical Phenomena"*, World Scientific (1984).

[60] F. Wegner, "Four-loop-order β-function of nonlinear σ-models in symmetric spaces" Nucl. Phys. **B316**, 663–678 (1989).

[61] S. Hikami, "Anderson localization in a superstring model representation" Physica **A167**, 149–162 (1990).

[62] S. Elitzur, "The Applicability of Perturbation Expansion to Two-dimensional

Goldstone Systems" Nucl. Phys. **B212**, 501–518 (1983).

[63] A.M. Finkel'stein, "Influence of coulomb interaction on the properties of disordered metals" Sov. Phys. JETP **57**(1), 97–108 (1983).

[64] A.M. Finkel'stein, "Weak Localization and Coulomb Interaction in Disordered Systems" Z. Phys. B **56**, 189–196 (1984).

[65] C. Castellani, C.D. Castro, and G. Forgacs, "Renormalizability of the density of states of interacting disordered electron system" Phys. Rev. B **30**(3), 1593–1598 (1984).

[66] C. Castellani, G. Kotliar, and P.A. Lee, "Fermi-Liquid Theory of Interacting Disordered Systems and the Scaling Theory of the Metal-Insulator Transition" Phys. Rev. Lett. **59**(3), 323–326 (1987).

[67] A.D. Zdetsis, C.M. Soukoulis, E.N. Economou, and G.S. Grest, "Localization in two- and three-dimensional systems away from the and center" Phys. · Rev. B **32**(12), 7811–7816 (1985).

[68] B.R. Bulka and B. Kramer, "Mobility Edge in the Three Dimensional Anderson Model" Z. Phys. B **60**, 13–17 (1985).

[69] B.R. Bulka, M. Schreiber and B. Kramer, "Localization, Quantum Interference, and the Metal-Insulator Transition" Z. Phys. B **66**, 21–30 (1987).

[70] D.C. Licciardello and E.N. Economou, "Study of localization in Anderson's model for random lattices" Phys. Rev. B **11**(10), 3697–3717 (1975).

[71] E.N. Economou, C.M. Soukoulis, and A.D. Zdetsis, "Localized states in disordered systems as bound states in potential wells" Phys. Rev. B **30**(4), 1686–1694 (1984).

[72] C.M. Soukoulis, A.D. Zdetsis, and N. Economou, "Localization in three-dimensional systems by a Gaussian random potential" Phys. Rev. B **34**(4), 2253–2257 (1986).

[73] E.A. Kotov and M.V. Sadovskii, "Self-Consistent Theory of Localization for the Anderson Model" Z. Phys. B **51**, 17–23 (1983).

Appendices

Appendix A: Power Counting

In this appendix, we examine the dimension of the physical variables. Based on the fact that the quantity such as $2\pi \int dr\, P(r) \cdot P(r)$ has the dimension of the energy, we find the following (canonical) dimensions. In the following, E and Λ denote the dimension of the energy and the momentum, respectively.

$$[P(r)] = \left[P_{k_r}\right] = E^{1/2}\Lambda^{d/2} \tag{A1}$$

$$[E(r)] = \left[E_l\right] = E^{1/2}\Lambda^{d/2} \tag{A2}$$

$$[\mu] = E^{1/2}\Lambda^{-d/2} \tag{A3}$$

Thus the canonical dimension of the linear and nonlinear susceptibilities are obtained as

$$\left[\chi^{(1)}\right] = E^0\Lambda^0, \tag{A4}$$

$$\left[\chi^{(3)}\right] = E^{-1}\Lambda^{-d}. \tag{A5}$$

Throughout this paper, we use the density of the states per volume N_0, which has the dimension like

$$[N_0] = E^{-1}\Lambda^d. \tag{A6}$$

The diffusion coefficient has the dimension of

$$[D_0] = E\Lambda^{-2}. \tag{A7}$$

Appendix B: RG treatment of the Anderson Localization

B.1 Introduction

In this appendix, we summarize the renormalization group (RG) treatment of the Anderson localization. The phase transition point (the mobility edge) between the localized phase and extended phase appears when the dimensionality of the system deviates from $d = 2$ to $d = 2 + \epsilon$ (ϵ is the positive infinitesimal) [57,58]. The localization problem and the critical behavior around the mobility edge is usually investigated by the renormalization group treatment within the frame of the field theoretical model called nonlinear sigma model by many authors [36–44,47,59]. Essentially their treatment is identical to the renormalization procedure of the diffusion modes themselves. Thus the similar treatment allows us to know the scaling behavior of $\Gamma_c(q,\omega)$ in the critical region (*i.e.* around the mobility edge.) The "self-energy correction" to the cooperon mode calculated in Sec. 5.2 corresponds to the one-loop calculation in the theory of the nonlinear sigma-model. The results of the higher loop corrections are already available [60,61]. In this Appendix, it is shown how the physical quantities can be evaluated by use of the renormalization group. We may leave to other references the detail about the mapping between the localization problem and the nonlinear sigma model.

B.2 Removal of Divergence by Dimensional Regulation

To go on along with the argument in the nonlinear sigma-model, we introduce the following parameters $t_0 = (\alpha N_0 D_0)^{-1}$ and $h_0 = (-i\omega + 2\gamma)(\beta D_0)^{-1}$, where D_0 is a bare diffusion coefficient. Numerical constants α and β will be defined later so as to absorb the numerical factors in the calculation. The canonical dimensions of these new parameters are $[t_0] = \Lambda^{2-d}$ and $[h_0] = \Lambda^2$. (The symbol Λ denotes the dimension of momentum, as in Appendix A.)

With these quantities, the bare diffusion propagator derived in Sec. 4.2 is expressed by

$$\Gamma_c^{(0)}(\boldsymbol{q}, \omega) = \frac{2\gamma'^2}{\pi N_0} \cdot \frac{1}{D_0 \boldsymbol{q}^2 - i\omega + 2\gamma} = \frac{2\gamma'^2}{\pi} \frac{\alpha t_0}{\boldsymbol{q}^2 + \beta h_0}. \tag{B1}$$

From the perturbational calculation done in Sec. 5.2, the lowest-order correction for the diffusion propagator is given in form of the self-energy $\Pi_c^{(1)}(\boldsymbol{q}, \omega)$, which is expressed by the new parameters as

$$\Pi_c^{(1)}(\boldsymbol{q}, \omega) = \frac{\boldsymbol{q}^2}{2\gamma'^2} \sum_{\boldsymbol{Q}} \frac{1}{\boldsymbol{Q}^2 + \beta h_0}. \tag{B2}$$

Then the renormalized cooperon mode at the lowest-order is

$$\Gamma_c^{(1)}(\boldsymbol{q}, \omega) = \left[\left(\Gamma_c^{(0)}(\boldsymbol{q}, \omega) \right)^{-1} - \Pi_c^{(1)}(\boldsymbol{q}, \omega) \right]^{-1} = \frac{2\gamma'^2 \alpha}{\pi} \frac{t_0}{(1 - \Delta')\boldsymbol{q}^2 + \beta h_0}, \tag{B3}$$

where

$$\Delta' = \frac{\alpha t_0}{\pi} \sum_{\boldsymbol{Q}} \frac{1}{\boldsymbol{Q}^2 + \beta h_0} = t_0 \frac{\alpha S_d \Gamma(\frac{d}{2})}{(2\pi)^{d+1}} (\beta h_0)^{\frac{d}{2}} \Gamma(\frac{-\epsilon}{2}), \tag{B4}$$

and S_d is the surface area of the d-dimensional unit sphere. Substitution of the value of $S_d = 2\pi^{d/2} / \Gamma(d/2)$ leads to

$$\Delta' = \frac{\alpha t_0}{\pi} \sum_{\boldsymbol{Q}} \frac{1}{\boldsymbol{Q}^2 + \beta h_0} = \frac{\alpha t_0}{\pi (4\pi)^{d/2}} (\beta h_0)^{\frac{\epsilon}{2}} \Gamma(\frac{-\epsilon}{2}). \tag{B5}$$

The correction term Δ' is proportional to t_0, but diverges at the limit of $\epsilon \to 0$

like ϵ^{-1}! The origin of this divergence at $\epsilon \to 0$ attributes to the short-distance singularity. In evaluation of Eq. (7) in Chapter 5, we introduce the ultra-violet cut-off $Q_c \sim \ell^{-1}$ to remove this singularity and obtain the correction Δ instead of Δ'. Here we take the alternative method to remove this short-distance singularity — the minimal substraction scheme to remove the dimensional pole.

It is well known that the two renormalization constants Z and Z_1 are enough to renormalize the theory of the nonlinear sigma model [42–44] such as

$$t_0 = \kappa^{-\epsilon} Z_1 t, \tag{B6}$$

$$h_0 = Z_1 Z^{-1/2} h, \tag{B7}$$

$$\frac{t_0}{h_0} = \kappa^{-\epsilon} \sqrt{Z} \frac{t}{h}, \tag{B8}$$

and define the renormalized vertex part by

$$\Gamma_c^{(1)}(\boldsymbol{q}, t, h, \kappa) \equiv Z^{-1} \, \Gamma_c^{(1)}(\boldsymbol{q}, t_0, h_0). \tag{B9}$$

Here the parameter κ has the dimension of the momentum. By substituting the renormalized parameters for the bare ones, it leads to

$$
\begin{aligned}
\left[\Gamma_c^{(1)}(\boldsymbol{q}, t, h, \kappa)\right]^{-1} &= Z \left[\Gamma_c^{(1)}(\boldsymbol{q}, t_0, h_0)\right]^{-1} \\
&= \frac{\pi}{2(\gamma')^2} \left[Z Z_1^{-1} \frac{\kappa^\epsilon \boldsymbol{q}^2}{\alpha t} + Z^{1/2} \frac{\kappa^\epsilon \beta h}{\alpha t} + \frac{Z \boldsymbol{q}^2 \, \Gamma(1 - \frac{\epsilon}{2})}{\pi (4\pi)^{d/2}} \frac{2}{\epsilon} \beta^{\epsilon/2} \left(Z Z_1^{-1/2} h \right)^{\epsilon/2} \right].
\end{aligned} \tag{B10}
$$

To absorb the divergence, we assume the forms of the renormalization constants like

$$Z = 1 + zt + O(t^2), \tag{B11}$$

$$Z_1 = 1 + z_1 t + O(t^2). \tag{B12}$$

It is a straightforward calculation that when the constants z and z_1 satisfy

$$z = 0, \tag{B13}$$

$$z_1 = \frac{2}{\epsilon} \cdot \frac{\alpha \beta^{\epsilon/2} \Gamma(1 - \frac{\epsilon}{2})}{\pi (4\pi)^{d/2}}, \tag{B14}$$

the dimensional pole is removed and we obtain the nondiverging cooperon mode which is defined by

$$\Gamma_c^{(1)}(\boldsymbol{q}, t, h, \kappa) = \frac{2\gamma'^2 \alpha}{\pi} \frac{\kappa^{-\epsilon} t}{(1 - \Delta') \boldsymbol{q}^2 + \beta h}, \tag{B15}$$

where

$$\Delta' = -t z_1 \{ (h\kappa^{-2})^{\epsilon/2} - 1 \}. \tag{B16}$$

For simplicity, we choose $\alpha \equiv \alpha_d = \pi(4\pi)^{d/2} / \Gamma(2 - \frac{d}{2})$ and $\beta = 1$. Then z_1 is equal to $\epsilon/2$. Setting the renormalization scale κ equal to the inverse of the mean free path ℓ^{-1} and taking the limit of $\epsilon \to 0$, we can confirm that the correction term Δ' exactly reproduces the result of Eq. (7) in Chapter 5:

$$\Delta' = -\lim_{\epsilon \to 0} t \frac{(h\kappa^{-2})^{\epsilon/2} - 1}{\epsilon/2} = \frac{1}{4\pi^2 N_0 D_0} \ln \left[\frac{2\gamma'}{-i\omega + 2\gamma} \right] = \Delta(\omega). \tag{B17}$$

B.3 Renormalization Group Equation for the Diffusion Propagator

Next we examine the universal scaling form of the cooperon mode. To do this, we write

$$\Gamma_c^{(1)}(\boldsymbol{q}, t, h, \kappa) \equiv \frac{2\gamma'^2 \alpha_d}{\pi} \Xi(\boldsymbol{q}, t, h, \kappa). \tag{B18}$$

Here $\Xi(\boldsymbol{q}, t, h, \kappa)$ is the diffusion propagator which has the dimension of Λ^d. In fact, this function $\Xi(\boldsymbol{q}, t, h, \kappa)$ is the coherent volume function introduced in Sec. 4.3. The function $\Xi(\boldsymbol{q}, t, h, \kappa)$ has the universal scaling form, which we will determine by use of the renormalization group treatment. Form the perturbational

treatment, which is justified in the small t limit, $\Xi(\boldsymbol{q},t,h,\kappa)$ has the form like

$$\Xi(q,t,h,\kappa) = \frac{\kappa^{-\epsilon}t}{\left\{1+\frac{2t}{\epsilon}\left[\left(h\kappa^{-2}\right)^{\epsilon/2}-1\right]+O(t^2)\right\}q^2+h}.\tag{B19}$$

The renormalization group equation is derived by the fact the bare function *i.e.*, $Z^{-1}\Xi(\boldsymbol{q},t,h,\kappa)$ is not explicitly dependent on κ with fixed bare parameters. Thus

$$\kappa\frac{d}{d\kappa}\left(Z^{-1}\Xi(\boldsymbol{q},t,h,\kappa)\right)\Big|_{t_0,h_0} = 0.\tag{B20}$$

We use the relation

$$\kappa\frac{d}{d\kappa}\Big|_{t_0,h_0} = \kappa\frac{\partial}{\partial\kappa}+\kappa\frac{\partial t}{\partial\kappa}\Big|_{t_0,h_0}\frac{\partial}{\partial t}+\kappa\frac{\partial h}{\partial\kappa}\Big|_{t_0,h_0}\frac{\partial}{\partial h}$$
$$= \kappa\frac{\partial}{\partial\kappa}+\beta(t)\frac{\partial}{\partial t}+\left(\frac{\zeta(t)}{2}+\frac{\beta(t)}{t}-\epsilon\right)h\frac{\partial}{\partial h},\tag{B21}$$

where the function $\beta(t)$ and $\zeta(t)$ is defined and calculated to the one-loop order as

$$\beta(t) \equiv \kappa\frac{\partial t}{\partial\kappa}\Big|_{t_0,h_0} = \epsilon t\cdot\left(1+\frac{\partial\ln Z_1}{\partial\ln t}\right)^{-1} = \epsilon t-2t^2+O(t^5),\tag{B22}$$

and

$$\zeta(t) \equiv \kappa\frac{\partial\ln Z}{\partial\kappa}\Big|_{t_0,h_0} = \beta(t)\frac{\partial\ln Z}{\partial t} = 0.\tag{B23}$$

Eventually we obtain the renormalization group equation for the diffusion propagator Ξ as

$$\left[\kappa\frac{\partial}{\partial\kappa}+\beta(t)\frac{\partial}{\partial t}+\zeta(t)+\left(\frac{\zeta(t)}{2}+\frac{\beta(t)}{t}-\epsilon\right)h\frac{\partial}{\partial h}\right]\Xi(\boldsymbol{q},t,h,\kappa)=0.\tag{B24}$$

Physically the meaning of Eqs. (B13) and (B23) is very important. In the nonlinear sigma model, the asymptotic behavior of the order parameter, say, σ is given [42,44,59] by

$$\sigma \sim (t-t^*)^{-\zeta(t^*)/2\beta'(t^*)}.\tag{B25}$$

According to Eq. (B23), the order parameter does *not* vanish at the transition point in the localization problem. This corresponds to the fact that the average density of state has no singularity around the mobility edge, so the relation $\zeta(t) = 0$ (*i.e.*, $Z = 1$) is expected to hold good even at the higher order calculation. In other words, the renormalization of the inelastic relaxation rate by disorder is not expected to exist. This is the reason we have considered only how the diffusion coefficient will be renormalized when we evaluate diffusion propagator, in Chapter 5. Eventually we obtain the renormalization group equation for the diffusion propagator as

$$\left[\kappa \frac{\partial}{\partial \kappa} + \beta(t) \frac{\partial}{\partial t} + \left(\frac{\beta(t)}{t} - \epsilon \right) h \frac{\partial}{\partial h} \right] \Xi(\boldsymbol{q}, t, h, \kappa) = 0. \tag{B26}$$

The solution of the equation above is easily obtained by the method of characteristics as

$$\Xi(\boldsymbol{q}, t, h, \kappa) = \Xi(\boldsymbol{q}, t(\rho), h(\rho), \kappa \rho^{-1}), \tag{B27}$$

where

$$\rho \frac{dt(\rho)}{d\rho} + \beta(t(\rho)) = 0, \tag{B28}$$

$$\rho \frac{dh(\rho)}{d\rho} + \left(\frac{\beta(t(\rho))}{t(\rho)} - \epsilon \right) h(\rho) = 0, \tag{B29}$$

and the initial conditions are given by $t(1) = t$ and $h(1) = h$. The solutions are easily obtained as (the critical exponent ν is given by $-1/\beta'(t^*)$):

$$t^* / t(\rho) = 1 \pm \left(\rho / \bar{\xi}(t) \right)^{1/\nu}, \qquad \begin{pmatrix} \text{delocalized} \\ \text{localized} \end{pmatrix} \tag{B30}$$

$$h(\rho) / t(\rho) = \rho^\epsilon \, h / t, \tag{B31}$$

where we introduce the (dimensionless) correlation length $\bar{\xi}(t) = |(t - t^*)/t|^{-\nu}$. The usual correlation length $\xi(t)$ will be defined by $\xi(t) = \ell \bar{\xi}(t)$.

B.3 Renormalization Group and Finite Size Effect

To consider the connection between the nonlinear sigma model and the length-dependent scaling theory [22], we consider the finite size effect of the sample. Since the renormalization procedure is to aim the removal of the short-distance singularity, the renormalization theory is not completely insensitive to the finite size effect. Consequently the renormalization equations are not modified, and the linear size of the sample L comes into the theory as a parameter. Thus we replace

$$\Xi(\boldsymbol{q},t,h,\kappa) \to \Xi_L(\boldsymbol{q},t,h,\kappa). \tag{B30}$$

Using the dimensional analysis such as $[\Xi] = \Lambda^{-d}$, we obtain

$$\begin{aligned}
\Xi_L(\boldsymbol{q},t,h,\kappa) &= \Xi_L(\boldsymbol{q},t(\rho),h(\rho),\kappa\rho^{-1}) \\
&= \Lambda^d \, \Xi_{L/\Lambda}(\Lambda\boldsymbol{q},t(\rho),\Lambda^2 h(\rho),\Lambda\kappa\rho^{-1}) \, .
\end{aligned} \tag{B31}$$

If we set $\Lambda = \rho = L / \ell$ and $\kappa = \ell^{-1}$, we can derive the relation between the different size as

$$\Xi_L(\boldsymbol{q},t,h) = \rho^d \, \Xi_\ell(\rho\boldsymbol{q},t(\rho),\rho^2 h(\rho))\Big|_{\rho=L/\ell}. \tag{B32}$$

In the case of the diffusion coefficient $N_0 D$, whose canonical dimension is Λ^ϵ, the same procedure can leads to the relation

$$L^\epsilon N_0 D_L(\boldsymbol{q},t,h) = \ell^\epsilon N_0 D_\ell(\rho\boldsymbol{q},t(\rho),\rho^2 h(\rho))\Big|_{\rho=L/\ell}. \tag{B33}$$

The equation above means the renormalization of the dimensionless conductance g_L! The relation given by Eq. (B33) is identical to the length-dependent scaling of Eq. (10) in Chapter 5, when the nonlinear sigma model is valid to describe the system. The theoretical drawback of the nonlinear sigma model results from the

fact that it deals with the transverse correlation function. In fact, q-dependence of the diffusion coefficient (*i.e.*, calculation of the critical exponent η) is rather problematic and can be done only by considering the invariant correlation function [40,47,62].

B.4 Relation between L_φ and $\tilde{L}_\varphi$

Using the relation of Eq. (B33), we can obtain the relation between L_φ and $\tilde{L}_\varphi$, which we have introduced in Sec. 5.3. In the sample size of the order of $\sim \ell$, the states are extended and the form of the correction term given by Eq. (B16) is expected to be valid. Thus we get

$$\ell^\epsilon N_0 D_\ell(\boldsymbol{q},t,h) = \frac{1}{t} + \frac{1}{t^*}\left\{(h\ell^2)^{\epsilon/2} - 1\right\}. \tag{B34}$$

Hence we estimate $D_L(\boldsymbol{q},t,h)$ as

$$L^\epsilon N_0 D_L(\boldsymbol{q},t,h) = \frac{1}{t(\rho)} + \frac{1}{t^*}\left\{(h(\rho)L^2)^{\epsilon/2} - 1\right\}. \tag{B35}$$

To make this expression valid, the term $\frac{t(\rho)}{t^*}\left\{(h(\rho)L^2)^{\epsilon/2} - 1\right\}$ must be small. For this reason, there arises a length scale which satisfies the condition

$$h(\rho)L^2 = 1. \tag{B36}$$

This length scale is what we have called $\tilde{L}_\varphi$ in Chapter 5, and relevant to the scaling theory of the diffusion coefficient. The condition of Eq. (B36) is transformed by use of Eqs. (B30) and (B31) like

$$h(\rho)(\tilde{L}_\varphi)^2 = \frac{t^*(\tilde{L}_\varphi / L_\varphi)^d}{1 + (\tilde{L}_\varphi / \xi)^\epsilon} = 1, \tag{B37}$$

in the delocalized phase. Thus we obtain

$$\begin{cases} \tilde{L}_\varphi \approx (t^*)^{-1/d} L_\varphi & (\text{ for } \xi \gtrsim L_\varphi) \\ \tilde{L}_\varphi \approx (t^*)^{-1/2} L_\varphi \sqrt{L_\varphi / \xi} & (\text{ for } \xi \lesssim L_\varphi) \end{cases} \tag{B38}$$

According to Eq. (B38), ω-dependence of $\tilde{L}_\varphi$ will change from $\sim \omega^{-1/2}$ to $\sim \omega^{-1/3}$ with the increasing of the correlation length ξ. This corresponds to the crossover behavior of the diffusion coefficient from $D(\omega) \sim \omega^{1/2}$ to $D(\omega) \sim \omega^{1/3}$.
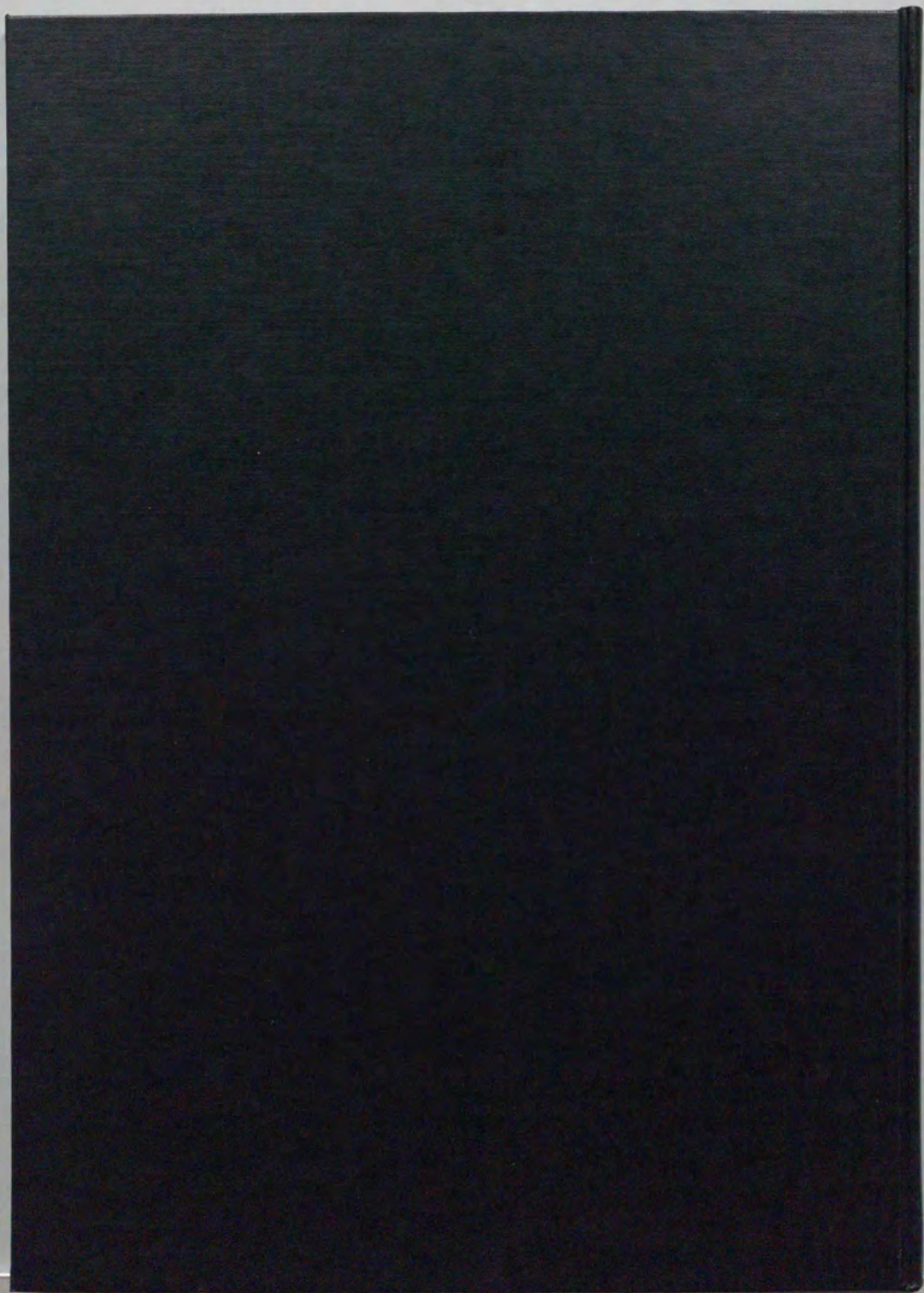
Kodak Color Control Patches

Blue Cyan Green Yellow Red Magenta White 3/Color Black

© Kodak, 2007 TM: Kodak

Kodak Gray Scale

A 1 2 3 4 5 6 M 8 9 10 11 12 13 14 15 B 17 18 19

C Y M

© Kodak, 2007 TM: Kodak